Mice carrying nonsense mutant p53 develop spontaneous tumors with frequent metastases

Running title: High tumor and metastases rate in *Trp53*^{R210X} mice

Charlotte Strandgren[1,2], Veronica Rondahl[2], Ann-Sophie Oppelt[1], Susanne Öhlin[1], Angelos Heldin[1], and Klas G. Wiman[1*]

[1]Karolinska Institutet, Dept. of Oncology-Pathology, Stockholm, Sweden

[2]Swedish University of Agricultural Sciences, Dept. of Animal Biosciences, Uppsala, Sweden

*Corresponding author: Klas Wiman; email: Klas.Wiman@ki.se

Conflict of interest

KGW is co-founder and shareholder of Aprea Therapeutics, a company that develops novel cancer therapy by targeting the DNA damage response pathway. KGW has previously received salary and research funding from Aprea Therapeutics. The other authors declare no conflicts of interest.

Abstract

The *TP53* tumor suppressor gene is mutated in a large fraction of human tumors. Close to 11% of *TP53* mutations are nonsense mutations, causing premature termination of protein synthesis and expression of truncated inactive p53 protein. The most common *TP53* nonsense mutation in human cancer is R213X. To study the impact of *TP53* nonsense mutations *in vivo*, we generated mice harboring the *Trp53* nonsense mutation R210X that corresponds to human *TP53* R213X. Initially, *Trp53*^{R210X} mice appear phenotypically normal, although the proportion of female *Trp53*$^{R210X/R210X}$ mice is dramatically reduced. Female homozygous mice are poor breeders and remain smaller and lighter than female heterozygous and wildtype littermates. *Trp53*$^{R210X/R210X}$ mice start to show tumors at 2.5 months of age, and their maximal lifespan is 8.5 months. *Trp53*$^{R210X/+}$ mice present tumors from 9 months of age, and by 16.5 months of age 50% of all heterozygous mice have developed overt tumors. 70% of tumors from *Trp53*$^{R210X/+}$ mice show loss of heterozygosity (LOH). The most common tumor type in homozygous mice is T-cell lymphoma, while soft-tissue sarcoma and osteosarcoma are the predominant tumor types in heterozygous mice. Although the *Trp53*^{R210X} tumor phenotype is comparable to those of *Trp53*-null and *Trp53*-missense knock-in mice, *Trp53*$^{R210X/R210X}$ mice develop frequent metastases and *Trp53*$^{R210X/+}$ mice have a longer overall survival than *Trp53*$^{R172H/+}$ missense mutant knock-in mice. Treatment of T-cell lymphoma cells from *Trp53*$^{R210X/R210X}$ mice with aminoglycoside G418 induces translational readthrough and expression of full-length functional p53. Our new unique mouse model will allow further studies of the effects of *Trp53* nonsense mutation in a multi-organ system and serve as a model for the Li-Fraumeni syndrome (LFS). It will also be valuable for preclinical evaluation of novel therapeutic strategies for targeting *TP53* nonsense mutations in cancer.

49

50 ## Introduction

51 The transcription factor p53 is activated by cellular stress (1). Activated p53 binds to
52 specific DNA motifs as a tetramer, transactivates multiple target genes (2, 3), and
53 controls e.g. cell cycle progression, DNA repair, metabolism, senescence, and
54 apoptosis (1, 4). The *TP53* gene is often inactivated in human tumors, most frequently
55 by missense mutations that disrupt p53 DNA binding and transactivation of target
56 genes (5, 6). Missense mutant p53 can inhibit co-expressed wildtype (WT) p53 through
57 a dominant-negative effect (DNE) that can increase resistance to genotoxic stress and
58 drive clonal selection (7). Some forms of missense mutant p53 may exert oncogenic
59 gain-of-function (GOF) activity, associated with a wider tumor spectrum and enhanced
60 invasion and metastasis (8-10). However, other studies have not found evidence for
61 mutant p53 GOF activity (7, 11, 12) and the concept of mutant p53 GOF remains
62 controversial. Around 11% of *TP53* mutations are nonsense mutations that result in a
63 premature stop codon (6) and expression of truncated p53 that lacks critical functional
64 domains and therefore fails to transactivate p53 target genes. Nevertheless, certain
65 truncated p53 proteins generated by *TP53* nonsense mutations may have oncogenic
66 properties (13).

67

68 Mouse models that either completely lack p53 or carry missense mutant p53 ($Trp53^{Mis}$)
69 support a key role of p53 as tumor suppressor. Homozygous *Trp53*-null or $Trp53^{Mis}$
70 mice show a striking cancer phenotype with a high rate of spontaneous tumors and
71 reduced survival compared to WT mice (9, 14-19). Both $Trp53^{-/-}$ and $Trp53^{Mis/Mis}$ mice
72 exhibit tumors from 3-6 months of age, whereas $Trp53^{+/-}$ and $Trp53^{Mis/+}$ mice display
73 tumors at 9-10 months of age, often associated with loss of the WT allele (loss of

74 heterozygosity, LOH). *Trp53*$^{-/-}$ and *Trp53*$^{Mis/Mis}$ mice mainly develop lymphomas and
75 sarcomas, whereas heterozygotes, especially the *Trp53*$^{Mis/+}$ models, also develop
76 carcinomas. *Trp53*$^{R172H/+}$ and *Trp53*$^{R270H/+}$ mice develop more invasive and metastasis
77 prone tumors compared to *Trp53*$^{+/-}$ mice, consistent with GOF activity for these
78 mutants (9, 16).
79
80 Mouse models designed to investigate the functional implications of *TP53* nonsense
81 mutations *in vivo* have previously not been established. Such models are crucial for a
82 better understanding of the impact of nonsense mutant p53 in a living organism, and
83 can also serve as platforms for preclinical development of pharmacological strategies
84 for therapeutic targeting of nonsense mutant *TP53* in cancer. Several compounds can
85 induce translational readthrough of nonsense mutant *TP53* and thus expression of full-
86 length and functional p53 protein in cultured cells, including G418 (20), Clitocine (21),
87 ELX-02 (22), 2,6-Diaminopurine (23), cc-90009 (24), and 5-Fluorouridine (25). Here
88 we present a novel mouse model carrying the *Trp53*-R210X nonsense mutation that
89 corresponds to *TP53*-R213X, the most common *TP53* nonsense mutation in human
90 tumors.
91

92 # Results

93 **Generation of a *Trp53*^{R210X} mouse model**

94 To generate a mouse model harboring the *Trp53*-R210X nonsense mutation, we used
95 CRISPR/Cas9 genome editing to introduce two single point mutations resulting in an
96 Arg (CGC) to STOP (TGA) substitution at codon 210 in exon 6 (Fig. 1A). The
97 CRISPR/Cas9 strategy was validated in NIH/3T3 mouse fibroblasts. Single-cell clones
98 of edited NIH/3T3 cells were genotyped as heterozygous using the introduced XbaI

99 cleavage site. PCR amplicons of *Trp53* exons 5-7 from the NIH/3T3 cell clones were
100 subcloned and sequencing of individual plasmid clones identified those carrying the
101 R210X mutation and the two downstream silent mutations. However, the XbaI site was
102 not present in all clones (Fig. 1B). ssODN template-triggered repair can generate short
103 conversion tracts of about 30 nucleotides with Gaussian-like distributions surrounding
104 the Cas9 cut site (26). The mutation producing the intended XbaI site was too far from
105 the Cas9 cut site and therefore outside of the effective conversion zone, explaining its
106 inconsistent introduction.
107
108 Genotyping the F0 offspring with PCR revealed that 6/17 pups were positive for the
109 R210X mutation. Sanger sequencing confirmed that two of the six pups also had the
110 XbaI site, whereas the remaining four lacked it (not shown). The pups were also
111 genotyped with restriction enzyme digestion, which confirmed the two pups carrying
112 the XbaI site, and also identified one pup carrying the XbaI site but not the correctly
113 mutated R210X sequence. The six F0 offspring carrying the correct R210X mutation
114 were set up for backcross breeding to WT C57BL/6J mice to eliminate possible off-
115 target events. Two founder animals, both lacking the XbaI site, generated F1 offspring,
116 and PCR genotyping verified germline transmission of the R210X allele (Fig. 1C).
117 Sequencing of 1049 bp surrounding the edited *Trp53* exon 6 locus confirmed clean
118 WT and R210X alleles in all F1 mice identified as heterozygous (Fig. 1D).
119
120 **Intercrosses of *Trp53*^{R210X} mice yield fewer and smaller female homozygous**
121 **offspring**
122 The *Trp53*^{R210X} strain was maintained by backcrossing *Trp53*$^{R210X/+}$ mice to WT
123 C57BL/6J mice. Backcross litter sizes at 2 weeks of age were normal compared to the

124 reference litter size of 7.0 pups for C57BL/6J mice (*informatics.jax.org*)
125 (Supplementary Table S1), and genotype and gender distribution (309 offspring) were
126 consistent with expected Mendelian inheritance but with significantly more WT males
127 (Supplementary Table S2). Different combinations of intercrosses were set up to
128 assess the viability and reproductive capacity of *Trp53*$^{R210X/R210X}$ mice (Supplementary
129 Table S1). Intercrossing only *Trp53*$^{R210X/R210X}$ mice resulted in litters with significantly
130 fewer pups at 2 weeks of age compared to backcrosses, whilst intercrosses with at
131 least one *Trp53*$^{R210X/+}$ mouse yielded similar litter sizes as the backcrosses
132 (Supplementary Table S1). Among all intercrosses between *Trp53*$^{R210X/R210X}$ and
133 *Trp53*$^{R210X/+}$ mice, only one litter was derived using a *Trp53*$^{R210X/R210X}$ female, yielding
134 a single male *Trp53*$^{R210X/+}$ pup. All other litters were spawned from *Trp53*$^{R210X/+}$
135 females. Thus, *Trp53*$^{R210X/R210X}$ female mice are fertile but have a reduced breeding
136 capacity.
137
138 Intercrosses between *Trp53*$^{R210X/+}$ and/or *Trp53*$^{R210X/R210X}$ mice gave fewer female
139 *Trp53*$^{R210X/R210X}$ offspring (Supplementary Table S2), whereas male offspring
140 distribution followed expected Mendelian inheritance regardless of genotype. Females
141 remained fewer when all *Trp53*$^{R210X/R210X}$ offspring were analyzed. Aside from the poor
142 breeding capacity of female *Trp53*$^{R210X/R210X}$ mice, heterozygous and homozygous
143 mice of both genders appeared phenotypically normal at young age and were fertile.
144
145 *Trp53*^{R210X} mouse bodyweights were recorded weekly from postnatal week 2 and until
146 euthanasia for all offspring from homozygous-generating intercrosses. Female
147 *Trp53*$^{R210X/R210X}$ mice had smaller body size (not shown) and were lighter than both WT
148 and *Trp53*$^{R210X/+}$ littermates at 2 weeks of age and remained lighter throughout life (Fig.

149 2A). In contrast, male mice had almost identical weight development regardless of
150 genotype until 34 weeks of age, when the remaining *Trp53*$^{R210X/R210X}$ males were
151 markedly lighter than their *Trp53*$^{R210X/+}$ and WT littermates, most likely due to
152 emaciation secondary to tumor growth (Fig. 2B).
153
154 **_Trp53_^{R210X} mice have a reduced lifespan**
155 The *Trp53*$^{R210X/R210X}$ mice had significantly shorter survival than *Trp53*$^{R210X/+}$ and WT
156 mice (adj. P-values: ***$p < 0.001$), as did *Trp53*$^{R210X/+}$ mice compared to WT (adj. P-
157 value: ***$p < 0.001$) (Fig. 2C-E). Female and male *Trp53*$^{R210X/R210X}$ mice had similar
158 survival, whilst female *Trp53*$^{R210X/+}$ mice had reduced survival compared to male (Fig.
159 2F). The apparent difference in survival between female and male WT mice was not
160 statistically significant ($p = 0.0573$). 11 male WT mice <1.5 years old were found dead
161 or were euthanized due to wounds or abdominal masses. Only one of these had
162 abdominal neoplasia; all others either showed no gross abnormalities or had enlarged
163 seminal vesicles, a normal phenomenon in aging male mice (27).
164
165 We also compared *Trp53*$^{R210X/R210X}$ survival to that of *Trp53*$^{R172H/R172H}$ missense knock-
166 in mice maintained in the same animal facility. The two mouse strains had strikingly
167 similar survival with a rapid decline from 3-8.5 months of age and similar mean survival:
168 145.5 days for *Trp53*$^{R210X/R210X}$ mice, 155 days for *Trp53*$^{R172H/R172H}$ mice (Fig. 2C-E). In
169 contrast, *Trp53*$^{R210X/+}$ mice survived longer than *Trp53*$^{R172H/+}$ mice, with mean survival
170 492 days and 460.5 days, respectively (Fig. 2E). There were no differences in survival
171 between female and male *Trp53*^{R172H} mice (Fig. 2G).
172
173 **Tumor development in _Trp53_^{R210X}–carrying mice is highly penetrant**

174 All animals, both euthanized and found dead, were necropsied, and histopathological
175 analysis was performed on available tissues from all *Trp53*$^{R210X/R210X}$ mice and a subset
176 of *Trp53*$^{R210X/+}$ and WT mice. Grossly visible tumors were found in 59 of 62 (95%)
177 *Trp53*$^{R210X/R210X}$ mice, 148 of 205 (72%) *Trp53*$^{R210X/+}$ mice, and 26 of 64 (41%) WT
178 mice. This confirms a highly penetrant tumor phenotype in *Trp53*^{R210X} mice.
179 Histopathological examination was performed on tissues from 49 *Trp53*$^{R210X/R210X}$ mice
180 (those with formalin-fixed tissues available) and 79 of the *Trp53*$^{R210X/+}$ mice with
181 suspected tumors that were also selected for LOH analysis (see below). To identify a
182 baseline for common tumors in the WT parents and siblings of the *Trp53*^{R210X} mutant
183 mice, we also examined tumors and tissues from the oldest of the available necropsied
184 WT mice (12 males, 12 females). Among the analyzed mice, 48 (98%) of the
185 *Trp53*$^{R210X/R210X}$ mice, 79 (100%) of the *Trp53*$^{R210X/+}$ mice, and 22 (92%) of the selected
186 WT mice had tumors (Supplementary Table S3).
187
188 **Different tumor spectra in *Trp53*$^{R210X/R210X}$ and *Trp53*$^{R210X/+}$ mice**
189 *Trp53*$^{R210X/R210X}$ mice only developed lymphomas and soft-tissue sarcomas (Fig. 3),
190 whereas *Trp53*$^{R210X/+}$ mice showed a broader tumor spectrum with osteosarcomas,
191 soft-tissue sarcomas, lymphomas, and carcinomas (Fig. 4A-D), as well as benign
192 tumors and a few tumors not further characterized (Supplementary Table S3). To
193 assess loss of the WT *Trp53* allele (LOH) in tumors from *Trp53*$^{R210X/+}$ mice, we
194 performed semi-quantitative PCR with the primers for genotyping (Fig. 4E). Out of 111
195 tumors from *Trp53*$^{R210X/+}$ mice analyzed, 78 (70%) showed LOH, consistent with a
196 selection pressure to eliminate the remaining WT allele.
197

198 *Trp53*$^{R210X/+}$ and WT mice showed similar tumor spectrum, apart from a unique
199 incidence of osteosarcomas observed only in *Trp53*$^{R210/+}$ mice (Fig. 5A). Lymphomas
200 were much more frequent in *Trp53*$^{R210/R210X}$ mice than in *Trp53*$^{R210X/+}$ and WT mice;
201 83% of the homozygous mice had lymphoma compared to only 37% of the
202 heterozygous mice ($p < 0.0001$) and 45% of WT mice ($p = 0.0041$). Primary lymphomas
203 occurred mainly in the thymus, spleen and lymph nodes (Fig. 5B). Since it was not
204 possible to differentiate between primary and metastatic splenic lymphomas, or
205 between primary and metastatic lymph node lymphomas, both spleen and lymph
206 nodes are referred to as primary sites. *Trp53*$^{R210X/R210X}$ mice developed predominantly
207 thymic lymphomas, and was the only genotype with metastasizing solitary thymic
208 lymphoma (Fig. 5B-C). Thymic lymphoma was less common in *Trp53*$^{R210X/+}$ mice (p =
209 0.0051), and absent in WT mice ($p = 0.0016$) (Fig. 5B).
210
211 *Trp53*$^{R210X/R210X}$ mice developed soft-tissue sarcomas in the skin, subcutis, and striated
212 muscle, whereas *Trp53*$^{R210X/+}$ mice developed this type of sarcoma in subcutis, liver,
213 spleen, seminal vesicles, lymph nodes, abdominal and mediastinal fat, lung, stomach,
214 pancreas and preputial gland (Figs. 3-4, and not shown). WT mice had soft-tissue
215 sarcomas in liver and lymph nodes (not shown). *Trp53*$^{R210X/+}$ male mice had a higher
216 incidence of soft-tissue sarcomas than females ($p = 0.0161$), while female *Trp53*$^{R210X/+}$
217 had more frequent osteosarcomas than males ($p < 0.0001$) (Fig. 5D).
218
219 To visualize the *in situ* distribution of lymphoma in a *Trp53*$^{R210X/R210X}$ mouse, we
220 performed post-mortem MRI on a 234-days old male that was euthanized due to a
221 large tumor on the ventral neck and respiratory distress. The MRI showed extensive

222 neoplasias originating and extending from the thymus and several lymph nodes (Fig.
223 5E-G).
224
225 We also characterized 22 thymic lymphomas, 16 splenic lymphomas and 17 soft-tissue
226 sarcomas from *Trp53*$^{R210X/R210X}$ mice by immunohistochemistry (IHC) (Supplementary
227 Table S4). CD3-staining confirmed T-cell origin of 4/4 female and 15/18 male thymic
228 tumors and all examined splenic tumors (3 female, 13 male). Vimentin-staining
229 confirmed mesenchymal origin of all soft-tissue sarcomas (2 female, 15 male). Desmin
230 staining demonstrated myocyte origin of 2/2 female and 13/15 male soft-tissue
231 sarcomas, and weak or no myogenin staining confirmed their classification as
232 rhabdomyosarcomas or myosarcomas. Two male soft-tissue sarcomas were negative
233 for desmin and myogenin, and were thus classified as soft-tissue sarcomas not further
234 specified. CD68 staining was used to identify histiocytic origin, and all positive cells
235 were non-neoplastic, infiltrating histiocytes or macrophages.
236
237 **Frequent lymphoma metastases in *Trp53*$^{R210X/R210X}$ mice**
238 Overall, 26 (54%) of the *Trp53*$^{R210X/R210X}$ mice, 22 (28%) of the *Trp53*$^{R210X/+}$ mice, and
239 3 (14%) of the WT mice had tumor metastases (Fig. 5A). *Trp53*$^{R210X/R210X}$ mice only
240 developed lymphoma metastases, and with higher frequency than *Trp53*$^{R210X/+}$ and WT
241 mice; 26 of 40 (65%) *Trp53*$^{R210X/R210X}$ mice with lymphoma in at least one primary site
242 developed metastases in at least one organ, as compared to 12 of 29 (41%) of the
243 *Trp53*$^{R210X/+}$ mice and 1 of 10 (10%) WT mice (Fig. 5C and Supplementary Table S3).
244 The most common lymphoma metastasis sites were lung and liver, followed by kidney,
245 heart, and submandibular salivary gland (not shown). Both number of metastases and
246 number of target organs are probably underestimated, since not all tissues were

247 sampled from all animals. *Trp53*$^{R210X/+}$ mice also had metastasizing soft-tissue
248 sarcoma, osteosarcoma, and carcinoma (Supplementary Table S3). Intriguingly, there
249 was no effect of metastatic disease on survival of *Trp53*$^{R210X/R210X}$ mice, and
250 *Trp53*$^{R210X/+}$ mice with metastatic disease had in fact longer survival than mice with no
251 metastasis (Fig. 6A). However, it should be noted that *Trp53*$^{R210X/+}$ mice with
252 osteosarcoma had significantly shorter survival than those with other types of tumors
253 (not shown); this may skew the survival data for mice without metastases since only
254 2/22 mice with osteosarcoma had metastasis. Furthermore, *Trp53*$^{R210X/R210X}$ mice with
255 thymic lymphoma had decreased survival compared to those with splenic and/or lymph
256 node lymphoma (Fig. 6B). Since thymic lymphoma can interfere with heart and lung
257 function, we investigated thymic tumor size. *Trp53*$^{R210X/R210X}$ mice with only thymic
258 lymphoma had the largest thymus tumors compared to mice with thymic lymphoma
259 and other primary tumors (Fig. 6C), and had the shortest survival (Fig. 6D). Thus,
260 solitary thymic lymphomas appear to have a higher growth rate than thymic
261 lymphomas that are concurrent with other lymphoma sites or soft-tissue sarcomas,
262 supporting the idea that solitary thymic lymphoma is a unique and *de novo* tumor
263 caused by the R210X mutation.
264

265 **Translational readthrough in T-cell lymphoma cells derived from *Trp53*$^{R210X/R210X}$**
266 **mice**

267 To investigate if translational readthrough of R210X nonsense mutant *Trp53* can
268 generate full-length active p53, we established T-cell lymphoma lines from thymic
269 lymphomas of *Trp53*$^{R210X/R210X}$ mice. Fig. 7A shows representative HE and CD3
270 immunohistochemistry staining of the thymus from one mouse, X405. Flow cytometry
271 with CD3, CD4 and CD8 antibodies verified T-cell origin, with 97.5% $CD3^+$ cells and

272 99% among those $CD4^+CD8^+$ (Fig. 7B). To examine translational readthrough, we
273 treated X405 T-cell lymphoma cells with aminoglycoside G418 for 72 h. We used
274 immunofluorescence staining with anti-p53 C-terminal antibody (280aa C-term) that
275 detects full-length p53 but not C-terminally truncated p53, and anti-p53 N-terminal
276 antibody N1 that detects both full-length and C-terminally truncated p53, to show that
277 100μM G418 induced full-length p53 (Fig. 7C). Western blotting with anti-p53 antibody
278 1C12, that recognizes an N-terminal epitope, confirmed a dose-dependent induction
279 of translational readthrough and expression of full-length p53 (Fig. 7D). We also found
280 a slight increase in truncated p53, most likely due to inhibition of nonsense-mediated
281 decay following translational readthrough. Moreover, qRT-PCR demonstrated that
282 induction of full-length p53 by G418 leads to upregulation of p53 target genes *Cdkn1a*
283 (p21), *Puma*, and *Zmat3* (Fig. 7E), as well as induction of apoptotic cell death as shown
284 by Annexin V staining (Fig. 7F), indicating that full-length p53 generated by
285 translational readthrough in these cells is fully functional as transcription factor.
286

287 # Discussion

288 We present here the first mouse model carrying a *Trp53* nonsense mutation. *Trp53*-
289 R210X corresponds to human *TP53*-R213X, one of the 10 most common *TP53*
290 mutations in human tumors. The *Trp53*^{R210X} allele was transferred at Mendelian
291 frequency in all crosses except intercrosses with female *Trp53*$^{R210X/R210X}$ mice that
292 resulted in smaller litters than the reference number for the C57BL/6J WT background
293 strain. These results are consistent with data from *Trp53*-null mice, where significant
294 decreases in embryonic implantation, pregnancy rate and litter size were observed in
295 matings with female *Trp53*$^{-/-}$ mice (28). This effect in *Trp53*-null mice is most likely

296 caused by reduced levels of leukemia inhibitory factor (LIF), which may also be
297 pertinent to our new *Trp53*^{R210X} strain.
298
299 We observed a substantial reduction in the frequency of female *Trp53*$^{R210X/R210X}$ pups
300 regardless of breeding setup, consistent with previous data for *Trp53*-null mice (29-
301 32). Exencephaly and craniofacial malformations in *Trp53*$^{-/-}$ female embryos (29, 30,
302 32) may also explain the skewed gender distribution observed in the *Trp53*$^{R210X/R210X}$
303 mice. Apart from the poor breeding capacity of female *Trp53*$^{R210X/R210X}$ mice,
304 heterozygous and homozygous mice of both genders appeared phenotypically normal
305 initially and were fertile, as reported for *Trp53*-null mice (14, 15).
306
307 The reduced bodyweights of female *Trp53*$^{R210X/R210X}$ mice compared to *Trp53*$^{R210X/+}$
308 and WT mice was unexpected. To our knowledge, similar findings have not been
309 reported for any genetically manipulated *Trp53*-model; in one study, female and male
310 *Trp53*$^{+/-}$ and *Trp53*$^{-/-}$ mice showed no difference in bodyweight (31), and two novel
311 *Trp53* missense knock-in mouse models displayed normal male and female
312 bodyweights (18). In our study, male mice of all three genotypes had almost identical
313 weight curves up until 34 weeks of age, very similar to those reported for male *Trp53*-
314 null mice (31). At that point, the weight curve for male *Trp53*$^{R210X/R210X}$ mice began to
315 deviate downward from those of *Trp53*$^{R210X/+}$ and WT mice, presumably a direct
316 consequence of tumor development.
317
318 *Trp53*$^{R210X/R210X}$ mice had similar survival curves as the control *Trp53*$^{R172H/R172H}$ mice,
319 as well as several other published *Trp53*-null and *Trp*53^{Mis} mouse models (9, 14-19,
320 31). Interestingly, *Trp53*$^{R210X/+}$ mice showed significantly longer survival than the

321 *Trp53*$^{R172H/+}$ mice in our colony. One plausible explanation for this difference is that the
322 truncated p53 protein encoded by the *Trp53*^{R210X} allele exerts a less pronounced
323 dominant-negative effect by oligomerization with co-expressed WT p53 as compared
324 to R172H missense mutant p53, or completely lacks such effect, allowing more potent
325 WT p53-dependent tumor suppression in *Trp53*$^{R210X/+}$ mice.
326
327 Whereas all homozygous *Trp53*^{R210X} mice had died or been euthanized by 8.5 months
328 of age, heterozygosity for the *Trp53*^{R210X} mutation did not affect survival until
329 approximately 9 months of age. As reported for homozygous *Trp53*-null and *Trp53*
330 missense knock-in mice (9, 14-19), homozygous *Trp53*^{R210X} mice showed a
331 remarkable susceptibility to tumor development at an early age, with lymphoma as the
332 predominant tumor type followed by soft-tissue sarcoma. This confirms that *Trp53*
333 nonsense mutation at codon 210 leads to a dramatically increased tumor incidence,
334 just like complete loss or missense mutation of *Trp53*. The heterozygous *Trp53*^{R210X}
335 mice also showed a striking tumor phenotype, with larger variation in tumor type, later
336 onset of clinical signs, and frequent LOH, again in agreement with previous studies of
337 *Trp53*-null and *Trp53* missense knock-in mice (9, 14-16, 19, 33). Thus, the *Trp53*$^{R210X/+}$
338 mice represent a new model for the Li-Fraumeni syndrome (LFS) in which *TP53*
339 nonsense mutations occur with a similar frequency as in somatic tumors (The *TP53*
340 Database (R20, July 2019): https://tp53.cancer.gov)(34).
341
342 We observed different tumor spectra in homozygous and heterozygous *Trp53*^{R210X}
343 mice, with early onset lymphomas and soft-tissue sarcomas in the *Trp53*$^{R210X/R210X}$
344 mice and a broader range of later onset tumors in the *Trp53*$^{R210X/+}$ mice, including
345 lymphomas, soft-tissue sarcomas, osteosarcomas and carcinomas, similar to the

346 range of tumors found in WT mice. The delayed tumor onset in *Trp53*$^{R210X/+}$ compared
347 to *Trp53*$^{R210X/R210X}$ mice reflects the need to eliminate the remaining WT allele. This
348 provides time for acquisition of additional genetic alterations that might predispose to
349 other tumor types. Moreover, the observed frequent thymic lymphomas in the
350 *Trp53*$^{R210X/R210X}$ mice but not in WT mice, along with the rapid growth of solitary thymic
351 lymphomas which resulted in earlier death or euthanasia of *Trp53*$^{R210X/R210X}$ mice,
352 suggest that thymic T-cell lymphoma is a *de novo* tumor in our model, as opposed to
353 early onset of a tumor that occurs naturally in the background strain. Similarly,
354 osteosarcomas were only found in the *Trp53*$^{R210X/+}$ mice and not in WT mice, indicating
355 that it too is a *de novo* tumor. Both thymic lymphoma and osteosarcoma are rare in
356 C57BL/6J mice (35, 36).
357
358 *Trp53*$^{R210X/R210X}$ mice frequently developed lymphoma metastases, most commonly to
359 liver and lung, but no soft-tissue sarcoma metastasis, whereas the *Trp53*$^{R210X/+}$ mice
360 showed a comparatively lower lymphoma and higher soft-tissue sarcoma metastasis
361 rate. Unexpectedly, metastatic disease did not have a negative effect on survival of
362 *Trp53*^{R210X} mice. This highlights the fact that even tumors that do not metastasize may
363 be life-threatening through various mechanisms, such as rapid growth that
364 compromises organ function, e.g. compression and restriction of heart and lungs by
365 thymic lymphomas, or production of substances that affect vital organs or have
366 detrimental systemic effects.
367
368 As far as we are aware, this is the first report of frequent and metastasizing lymphoma
369 in genetically engineered *Trp53* mutant mice. The high rate of metastasis in *Trp53*^{R210X}
370 mice, which is in contrast to data for *Trp53*$^{R246S/R246S}$, *Trp53*$^{R245W/R245W}$ and

371 *Trp53*$^{R270H/R270H}$ mice that only infrequently or never develop metastasis (17, 19),
372 suggests that truncated p53 derived from the R210X nonsense mutant allele can exert
373 some kind of GOF activity. Indeed, GOF features of C-terminally truncated p53
374 proteins have been demonstrated in cell culture and *in vivo* assays (13). However, we
375 did not observe any significant differences in overall survival, tumor incidence, tumor
376 spectrum or LOH frequency between our *Trp53*^{R210X} mice and data reported for *Trp53*-
377 null mice (14, 15, 33), arguing against a prominent GOF activity of the R210X allele in
378 this setting. A caveat is that data on metastasis frequency in homozygous *Trp53*-null
379 or missense knock-in mice are scarce in previous studies (9, 14-19). Thus, we do not
380 exclude that further investigation will reveal GOF properties of nonsense mutant *TP53*.
381
382 In conclusion, our *Trp*53^{R210X} mouse model should facilitate the development of novel
383 strategies for therapeutic targeting of nonsense mutant *TP53* in cancer. Importantly,
384 we have confirmed that induction of translational readthrough of the *Trp53*-R210X
385 allele in mouse thymic lymphoma cells results in the expression of full-length and
386 functional p53 protein and cell death by apoptosis. Further studies of downstream
387 effects of p53 activation in these cells are required, and it will also be interesting to
388 examine translational readthrough and p53 activation in cell lines derived from other
389 types of tumors in *Trp53*^{R210X} mice. Induction of translational readthrough is a potential
390 therapeutic strategy for nonsense mutant *TP53*-carrying tumors upon diagnosis, or for
391 prevention of tumors in cancer-prone individuals such as LFS family members carrying
392 an inherited *TP53* nonsense mutation. Given that around 11% of all *TP53* mutations in
393 cancer are nonsense mutations (6), successful clinical implementation of efficient
394 readthrough-inducing therapy would have a significant impact on public health
395 worldwide.

396

397 # Materials and methods

398 **Generation of *Trp53*^{R210X} mutant mice**

399 To generate the *Trp53*^{R210X} mouse model, a chemically modified synthetic single-guide
400 RNA (sgRNA) (5'-gcagacttttCGCcacagcg-3') with an 80-mer SpCas9 scaffold targeting
401 the region encoding the R210 codon in *Trp53* exon 6 was used (CRISPRevolution
402 sgRNA EZ Kit, Synthego, USA). Single strand oligodeoxynucleotides (ssODNs) of 200
403 nucleotides were used as repair template (Ultramer™, Integrated DNA Technologies,
404 USA; 5'-
405 ctgacttattcttgctcttaggcctggctcctccccagcatcttatccgggtggaaggaaatttgtatcccgagtatctAga
406 agacaggcagacttttTgAcaTagTgtggtggtaccttatgagccacccgaggtctgtaattttgttttggtttgtgcgtct
407 tagagacagttgactccagcctagactgatgttgac-3') for homology-directed repair (HDR). The
408 sequence included silent mutations to exclude recutting of the guide RNA and an XbaI
409 site (tctAga) close to the R210X codon TgA to facilitate genotyping. The CRISPR/Cas9
410 strategy was verified by editing NIH/3T3 mouse fibroblasts (CRL-1658, ATCC, USA),
411 see below for genotyping strategy using the XbaI site. The edited NIH/3T3 cells were
412 plated as single cells and cultured in Dulbecco's Modified Eagle's Medium High
413 Glucose (DMEM) supplemented with 5% FBS.

414

415 The edited mice were produced at the Karolinska Center for Transgene Technologies,
416 Karolinska Institutet. Zygotes harvested from superovulated and mated C57BL/6J
417 female mice (Charles River Laboratories, Germany) were microinjected into the
418 pronuclei with injection buffer [10 mM Tris-HCl (pH 7.5), 0.1 mM EDTA] containing a
419 pre-formed Cas9-sgRNA ribonucleoprotein complex at a concentration of 20 ng/µl
420 eSpCas9 (Sigma-Aldrich/Merck, Germany), 20 ng/µl of the *Trp53* sgRNA (Synthego),

421 and 20 ng/µl of the 200 nucleotide ssODN Ultramer (Integrated DNA Technologies).
422 Microinjected zygotes were implanted into oviducts of pseudopregnant SOPF
423 RjOrl:SWISS (Janvier Labs, France) surrogate female mice via microsurgery. Ear
424 punch biopsies from the F0 offspring were lysed (37) and subjected to PCR with
425 primers encompassing the edited region, giving a 1049 bp amplicon (*Trp53* exon 5-7;
426 Forward primer: 5'-ATCGTTACTCGGCTTGTCCC-3'; Reverse primer: 5'-
427 GGGTAGGAACCAAAGAGCGT-3'). PCR products were purified using the QIAquick
428 PCR Purification Kit (Qiagen, Germany) and digested with restriction enzyme XbaI
429 (New England Biolabs, USA) to reveal recombination of the ssODN template. The PCR
430 amplicons from selected candidate F0 mice were subcloned into pMiniT 2.0 (New
431 England Biolabs) and individual plasmid clones were subjected to Sanger sequencing
432 (KIGene, Karolinska Institutet). All F1 mice identified as heterozygous were further
433 confirmed by Sanger sequencing individual plasmid clones using primers described
434 above for *Trp53* exon 5-7. Sequences were analyzed using the SnapGene (version
435 7.0.1) and Jalview (version 2.11.2.6) softwares.
436
437 **Animal studies**
438 Animal care was in accordance with Swedish regulation and Karolinska Institutet
439 guidelines. Experimental mice were housed in enriched individually ventilated cages
440 in 1 hour dawn/dusk and 10h light/dark cycle, at 22°C ± 2°C and 50% ± 20% air
441 humidity at a pathogen-free animal facility at Karolinska Institutet. Mice were supplied
442 with irradiated CRM(P) mouse pellets (SAFE Diets, France) and drinking water *ad*
443 *libitum*. All animal studies were approved by the Stockholm Regional Animal Ethical
444 Committee, Sweden (Dnr 14188-2019).
445

446 *Trp53*$^{R210X/+}$ mice were maintained on a C57BL/6J background by backcrossing to
447 C57BL/6J mice purchased from Charles River Laboratories. Homozygous mice were
448 generated by intercrossing *Trp53*$^{R210X/+}$ and/or *Trp53*$^{R210X/R210X}$ mice. *Trp53*^{R172H} (9)
449 (C57BL/6J background), a kind gift from Dr Guillermina Lozano, MD Anderson Cancer
450 Center, Houston, were used as a reference strain. DNA for genotyping was extracted
451 from ear biopsies using the Gentra Puregene Tissue Kit (Qiagen). Genotyping
452 *Trp53*^{R210X} mice was performed by two separate touchdown PCR reactions (10 cycles
453 of touchdown from 65°C to 61°C, followed by 25 cycles at 60°C – total 35 cycles) with
454 specific primers to detect mutant and WT alleles, respectively (*Trp53*-R210X allele,
455 252 bp amplicon, forward primer: 5'-CATCTACAAGAAGTCACAGCAC-3', reverse
456 primer: 5'-GGTACCACCACACTATGTCA-3'; *Trp53*-R210 WT allele, 95 bp amplicon,
457 forward primer: 5'-GCAGACTTTTCGCCACAGC-3', reverse primer: 5'-
458 CTGGAGTCAACTGTCTCTAAGAC-3'). PCR products w*ere* analyzed on 2% agarose
459 gels. Genotyping of *Trp53*^{R172H} mice was performed as described(9). Mice presenting
460 a mutant allele band together with a WT allele band in the genotyping PCR were
461 considered heterozygous, and mice showing only a mutant allele band and no WT
462 band were considered homozygous. Mice from *Trp53*$^{R210X/+}$ intercrosses that were
463 negative for the R210X mutation are referred to as WT mice and were used as controls.
464 *Trp53*^{R210X} mouse bodyweights were recorded weekly from postnatal week 2 and until
465 moribund and euthanized. Homozygous mice were palpated weekly for tumor
466 occurrence starting at 10 weeks of age, and heterozygous as well as WT littermate
467 mice were palpated from 12 months of age.
468
469 **Tissue collection and processing**

470 Moribund mice were euthanized by cervical dislocation and tissues were directly
471 collected for further analysis. Tissue samples were also collected from mice found
472 dead, unless there was too much autolysis. Tissues for molecular analysis were
473 collected either by immediate snap freezing in liquid nitrogen and stored at -80°C, or
474 in RNAlater™ Stabilizing Solution (Thermo Fisher Scientific, USA). Tissues collected
475 for histological analysis were carefully dissected and fixed in 4% formaldehyde
476 (buffered, pH 6.9, Sigma-Aldrich/Merck) at room temperature on a slow set rocking
477 table for 24-48h, and subsequently transferred to 70% ethanol for storage at 4°C until
478 further use. Skeletal tissues and calcified tumors were decalcified using MolDecal10
479 Ready to use Solution (pH 7.2-7.4, HistoLab Products, Sweden) for 3-4 weeks in 4°C
480 on a slow set rocking table. Decalcification solution was changed every 3-5 days. For
481 establishment of thymic lymphoma cell lines, enlarged thymuses from homozygous
482 mice were fine dissected and collected in ice-cold PBS (see below).
483
484 **Histopathology and immunohistochemistry (IHC)**
485 Formaldehyde-fixed tissues were processed in an automated tissue processing
486 machine (LOGOS, Milestone Medical, Italy) for dehydration, followed by paraffin-
487 embedding and microtome sectioning (4μm). Sections were collected on Superfrost™
488 Plus Adhesion Microscope Slides (Thermo Scientific, USA). For histological analysis,
489 slides were stained with hematoxylin and eosin (HE) using a standard protocol.
490 Determination of tumor type was performed by IHC following standard methods.
491 Staining was performed with antibodies against CD3 (1:900, A0452,
492 DAKO/Technologies, USA), desmin (1:2000, ab32362, Abcam, UK), myogenin (1:100,
493 ab124800, Abcam) (all with EDTA pH 8.5 for antigen retrieval), CD68 (1:800, #97778,
494 Cell Signaling Technology, USA), and vimentin (1:1000, ab92547, Abcam) (both with

495 citrate buffer pH 6.0 for antigen retrieval), and incubation at 4°C overnight.
496 Visualization was performed using ImmPress HRP and ImmPACT DAB kits (MP-7401
497 and SK-4205, Vector Laboratories, USA), followed by counterstaining in Mayer's
498 hematoxylin. HE and IHC slides were examined by light microscopy.
499
500 ***Ex vivo* MRI data acquisition**
501 MRI data were acquired using a 9.4T MRI scanner (Varian, UK) with a horizontal bore.
502 The scanner was controlled with software VnmrJ v4.0 Revision A. A gradient insert
503 with an inner diameter of 12 cm (Varian, UK) and a millipede RF-coil with an inner
504 diameter of 40 mm (Varian) were used. The scan program contained an overview scan,
505 scanner alignment, diffusion weighted, T1-weighted (fat suppressed and Two-point
506 Dixon) and T2-weighted (fat suppressed and FLAIR) scans. Overview and Two-point
507 Dixon sequences were acquired in sagittal plane, the others in dorsal plane. Images
508 were reviewed in collaboration with a European specialist in veterinary diagnostic
509 imaging on a computer workstation using digital imaging and communications in
510 medicine image viewing software (Horos software vers. 3.3.6, Horos project).
511
512 **Assessment of loss of heterozygosity (LOH)**
513 *Trp53*$^{R210X/+}$ tumors were analyzed for LOH by a semi-quantitative method, using the
514 aforementioned genotyping PCR but with only 29 cycles and 100ng DNA per sample.
515 DNA was extracted as described above under Animal studies. For each tumor, tail
516 tissue from the corresponding mouse was used as a control. To quantify the fraction
517 of WT allele left in the tumor, agarose gel band intensities of WT and mutant PCR
518 products were measured for tail and tumor tissue, respectively. Tumor intensity ratio
519 was normalized to the respective tail using the following formula:

520 $$\frac{tumorWT/tumorMUT}{tailWT/tailMUT}$$

521 LOH was defined as a value < 0.5, indicating <50% WT allele fraction in tumor
522 compared to tail.
523
524 **Establishment of T-cell lymphoma cell lines**
525 Thymic (T-cell) lymphoma cell lines were established and cultured as described (38).
526
527 **Flow cytometry**
528 T-cell origin of established cell lines was verified by flow cytometry. $5x10^5$ cells were
529 incubated in staining buffer (3% FBS in PBS) containing the following antibodies: Anti-
530 CD3-FITC (1:100, #11-0031-85), Anti-CD4-APC (1:100, #17-0041-83), and Anti-CD8-
531 PE (1:100, #12-0081-85) (all eBioScience, USA). Alive cells were assessed by
532 FxCycle™ Violet Stain DAPI (Thermo Fisher Scientific) diluted 1:500 in staining buffer.
533 Cells were incubated 20 min at 4˚C with 100µl of the antibody/DAPI cocktail, followed
534 by adding 1ml staining buffer and centrifugation at 400g for 5 min. Cells were
535 resuspended in 500µl staining buffer, filtered through a 35µm cell strainer and analyzed
536 using a NovoCyte flow cytometer (ACEA Biosciences, USA).
537
538 Cell death was assessed by Annexin V staining. $5x10^4$ cells/ml were seeded in 6-well-
539 plates using 4ml/well. Cells were treated with G418 (0-200µM) for 72 hours. Treated
540 cells were harvested, washed with DPBS (Sigma-Aldrich/Merck), resuspended in
541 Annexin V binding buffer, counted using Countess 3 Automated Cell Counter (Thermo
542 Fisher Scientific) and diluted to $1x10^6$ cells/ml. 100µl cell dilution was incubated with
543 5µl BD HorizonTM V450 Annexin V antibody (BD Biosciences, USA) for 15 minutes in

544 the dark at room temperature (RT). 400µl Annexin V binding buffer was added and
545 cells were analyzed using a NovoCyte flow cytometer (ACEA Biosciences).
546
547 **Western blotting**
548 T-lymphoma cells were seeded in 6-well-plates at 1-3x10^5 cells/ml and treated with
549 G418 (0-200µM) for 72 hours. Western blotting was performed as previously described
550 using 80µg protein (39). Detection of p53 was performed using primary antibody 1C12
551 anti-p53 (1:1000, #2524, Cell Signaling Technology) and an HRP-conjugated Rabbit-
552 anti-Mouse IgG secondary antibody (1:5000, #61-6520, Invitrogen, USA). Following
553 visualization of p53, HRP-conjugated G-9 anti-GAPDH antibody (1:10 000, sc-365062,
554 Santa Cruz Biotechnology, USA) was used as a loading control. Proteins were
555 visualized by SuperSignal™ West Femto Maximum Sensitivity Substrate and iBright
556 FL1000 imaging system (both Thermo Fisher Scientific). All original Western blots are
557 provided in Supplementary Information.
558
559 **Immunofluorescence staining**
560 1x10^5 T-lymphoma cells in 100µl PBS were used for Cytospin (Shandon CYTOSPIN
561 4, Thermo Electron Corporation) at 1500 rpm for 1 min. Cells were fixed in 4%
562 formaldehyde for 10 min at RT, permeabilized using 0.1% Triton in PBS for 5 min at
563 RT, followed by washing in PBS. Primary antibodies rabbit polyclonal p53 N-terminal
564 antibody [N1] (GTX100629, Genetex, USA) and goat polyclonal Anti-TP53 (280aa C-
565 Term) (ASJ-VN4O74-150, Nordic Biosite, Sweden) were diluted together at 1:100 in
566 PBS, incubation 4°C ON. Following PBS wash, secondary antibodies Donkey anti-
567 Rabbit IgG (H+L) Alexa Fluor™ Plus 488 (A32790) and Donkey anti-Goat IgG (H+L)
568 Alexa Fluor™ Plus 555 (A32816) (both Thermo Fisher Scientific) were diluted together

569 at 1:1000 in PBS, incubation 1h in RT. Slides were washed with PBS and mounted
570 with Fluoroshield™ containing DAPI (F6057, Sigma-Aldrich/Merck). An AxioObserver
571 Z1 (Zeiss) microscope was used for imaging.
572
573 **Quantitative real-time PCR (qRT-PCR)**
574 T-lymphoma cells were seeded in 6-well-plates at $5x10^4$ cells/ml and treated with G418
575 (0-200μM) for 72 hours. Cells were harvested and RNA extraction, cDNA synthesis
576 and qRT-PCR were performed as described except that cDNA synthesis was carried
577 out using SuperScript IV (Thermo Fisher Scientific) (25). TaqMan probes used were
578 *p53* (*Trp53*; Mm01731290_g1), *p21* (*Cdkn1a*; Mm00432448_m1), *Puma* (*Bbc3*;
579 Mm00519268_m1), *Zmat3* (Mm00494181_m1), and *Gapdh* (Mm99999915_g1).
580
581 **Statistical analysis**
582 Statistical analysis of numerical data was performed using GraphPad Prism 10
583 (version 10.4.0). Multiple groups were compared using One-way ANOVA, followed by
584 Tukey's multiple comparisons test when all groups were compared to each other, or
585 by Dunnett's multiple comparisons test when all groups were compared to only the
586 control group. Chi-square goodness-of-fit test was used to assess Mendelian
587 inheritance patterns of gender and genotypes. Mouse bodyweight growth curves were
588 analyzed by Mixed-effects analysis with Tukey's multiple comparisons test. Kaplan-
589 Meier mouse survival curves were analyzed by log-rank (Mantel-Cox) test followed by
590 correction for multiple comparisons using the Holm-Šídák method. Statistical
591 significance was defined as $p < 0.05$. Values are presented as mean ± SEM.
592 Statistical analysis of non-numerical data was performed using R (version 4.2.2) via
593 BioRender Graph. Mann-Whitney U test was used for gender comparisons within

genotypes. Kruskal-Wallis test with Dunn's multiple comparisons test was used for genotype comparisons. Statistical significance was defined as $p < 0.05$.

Acknowledgements

We thank Bernhard Schmierer, Karolinska Genome Engineering (KGE) core facility, and Stephan Teglund, Karolinska Center for Transgene Technologies (KCTT), for expert help with generation of the *Trp53*^{R210X} mouse strain, Anna Malmerfelt at the Histology core facility, Dept. Of Oncology-Pathology, for excellent help with preparation of sections and staining for histopathological analysis, and Alexis Gombert (DVM, IPSAV, ECVDI Diplomate), at the Diagnostic Imaging Clinic, University Animal Hospital, Swedish University of Agricultural Sciences, for expert help with interpreting and describing the MRI results.

Author contribution

CS, VR, SÖ, AH and KGW designed the experiments. CR, VR, AH, SÖ and ASO performed the experiments. All authors took part in analysis and interpretation of data. CS, VR, AH and KGW wrote the manuscript. KGW acquired funding for the project.

Ethics

All animal studies were approved by the Stockholm Regional Animal Ethical Committee, Sweden (Dnr 14188-2019).

Funding

618 This work was supported by grants to KGW from European Research Council
619 (Advanced ERC grant No. 694825-TRANSREAD), the Swedish Research Council (VR
620 2017-01509; 2021-02064), the Swedish Cancer Fund (Cancerfonden 18 0774; 21
621 1473 Pj 01 H), the Swedish Childhood Cancer Fund (Barncancerfonden PR2020-
622 0042), and Karolinska Institutet.

623

624 ## Data availability

625 All original data are available upon request. This work does not include any datasets,
626 such as DNA sequences or protein structure data, that have been uploaded in publicly
627 available repositories.

628

629 # References

630 1. Mello SS, Attardi LD. Deciphering p53 signaling in tumor suppression. Curr Opin Cell
631 Biol. 2018;51:65-72.

632 2. Vousden KH, Prives C. Blinded by the Light: The Growing Complexity of p53. Cell.
633 2009;137(3):413-31.

634 3. Andrysik Z, Galbraith MD, Guarnieri AL, Zaccara S, Sullivan KD, Pandey A, et al.
635 Identification of a core TP53 transcriptional program with highly distributed tumor
636 suppressive activity. Genome Res. 2017;27(10):1645-57.

637 4. Kastenhuber ER, Lowe SW. Putting p53 in Context. Cell. 2017;170(6):1062-78.

638 5. Joerger AC, Ang HC, Fersht AR. Structural basis for understanding oncogenic p53
639 mutations and designing rescue drugs. Proceedings of the National Academy of Sciences of
640 the United States of America. 2006;103(41):15056-61.

641 6. Tate JG, Bamford S, Jubb HC, Sondka Z, Beare DM, Bindal N, et al. COSMIC: the
642 Catalogue Of Somatic Mutations In Cancer. Nucleic Acids Res. 2019;47(D1):D941-D7.

643 7. Boettcher S, Miller PG, Sharma R, McConkey M, Leventhal M, Krivtsov AV, et al. A
644 dominant-negative effect drives selection of TP53 missense mutations in myeloid
645 malignancies. Science. 2019;365(6453):599-604.

646 8. Oren M, Rotter V. Mutant p53 gain-of-function in cancer. Cold Spring Harb Perspect
647 Biol. 2010;2(2):a001107.

648 9. Lang GA, Iwakuma T, Suh YA, Liu G, Rao VA, Parant JM, et al. Gain of function of a p53
649 hot spot mutation in a mouse model of Li-Fraumeni syndrome. Cell. 2004;119(6):861-72.

650 10. Muller PA, Caswell PT, Doyle B, Iwanicki MP, Tan EH, Karim S, et al. Mutant p53 drives
651 invasion by promoting integrin recycling. Cell. 2009;139(7):1327-41.

652 11. Lane DP. Mutant p53 Gain-of-Function in the Spotlight: Are We Suffering a GOF
653 Delusion? Cancer Discov. 2024;14(2):211-3.

654 12. Wang Z, Burigotto M, Ghetti S, Vaillant F, Tan T, Capaldo BD, et al. Loss-of-Function but
655 Not Gain-of-Function Properties of Mutant TP53 Are Critical for the Proliferation, Survival, and
656 Metastasis of a Broad Range of Cancer Cells. Cancer Discov. 2024;14(2):362-79.

657 13. Shirole NH, Pal D, Kastenhuber ER, Senturk S, Boroda J, Pisterzi P, et al. TP53 exon-6
658 truncating mutations produce separation of function isoforms with pro-tumorigenic
659 functions. Elife. 2016;5.

660 14. Donehower LA, Harvey M, Slagle BL, McArthur MJ, Montgomery CA, Jr., Butel JS, et al.
661 Mice deficient for p53 are developmentally normal but susceptible to spontaneous tumours.
662 Nature. 1992;356(6366):215-21.

663 15. Jacks T, Remington L, Williams BO, Schmitt EM, Halachmi S, Bronson RT, et al. Tumor
664 spectrum analysis in p53-mutant mice. Curr Biol. 1994;4(1):1-7.

665 16. Olive KP, Tuveson DA, Ruhe ZC, Yin B, Willis NA, Bronson RT, et al. Mutant p53 gain of
666 function in two mouse models of Li-Fraumeni syndrome. Cell. 2004;119(6):847-60.

667 17. Lee MK, Teoh WW, Phang BH, Tong WM, Wang ZQ, Sabapathy K. Cell-type, dose, and
668 mutation-type specificity dictate mutant p53 functions in vivo. Cancer Cell. 2012;22(6):751-
669 64.

670 18. Gencel-Augusto J, Su X, Qi Y, Whitley EM, Pant V, Xiong S, et al. Dimeric p53 Mutant
671 Elicits Unique Tumor-Suppressive Activities through an Altered Metabolic Program. Cancer
672 Discov. 2023;13(5):1230-49.

673 19. Xiong S, Chachad D, Zhang Y, Gencel-Augusto J, Sirito M, Pant V, et al. Differential Gain-
674 of-Function Activity of Three p53 Hotspot Mutants In Vivo. Cancer Res. 2022;82(10):1926-36.

675 20. Floquet C, Deforges J, Rousset JP, Bidou L. Rescue of non-sense mutated p53 tumor
676 suppressor gene by aminoglycosides. Nucleic Acids Res. 2011;39(8):3350-62.

677 21. Friesen WJ, Trotta CR, Tomizawa Y, Zhuo J, Johnson B, Sierra J, et al. The nucleoside
678 analog clitocine is a potent and efficacious readthrough agent. RNA. 2017;23(4):567-77.

679 22. Crawford DK, Alroy I, Sharpe N, Goddeeris MM, Williams G. ELX-02 Generates Protein
680 via Premature Stop Codon Read-Through without Inducing Native Stop Codon Read-Through
681 Proteins. J Pharmacol Exp Ther. 2020;374(2):264-72.

682 23. Trzaska C, Amand S, Bailly C, Leroy C, Marchand V, Duvernois-Berthet E, et al. 2,6-
683 Diaminopurine as a highly potent corrector of UGA nonsense mutations. Nat Commun.
684 2020;11(1):1509.

685 24. Baradaran-Heravi A, Balgi AD, Hosseini-Farahabadi S, Choi K, Has C, Roberge M. Effect
686 of small molecule eRF3 degraders on premature termination codon readthrough. Nucleic
687 Acids Res. 2021;49(7):3692-708.

688 25. Palomar-Siles M, Heldin A, Zhang M, Strandgren C, Yurevych V, van Dinter JT, et al.
689 Translational readthrough of nonsense mutant TP53 by mRNA incorporation of 5-
690 Fluorouridine. Cell Death Dis. 2022;13(11):997.

691 26. Kan Y, Ruis B, Takasugi T, Hendrickson EA. Mechanisms of precise genome editing using
692 oligonucleotide donors. Genome Res. 2017;27(7):1099-111.

693 27. Pettan-Brewer C, Treuting PM. Practical pathology of aging mice. Pathobiol Aging Age
694 Relat Dis. 2011;1.

695 28. Hu W, Feng Z, Teresky AK, Levine AJ. p53 regulates maternal reproduction through LIF.
696 Nature. 2007;450(7170):721-4.

697 29. Sah VP, Attardi LD, Mulligan GJ, Williams BO, Bronson RT, Jacks T. A subset of p53-
698 deficient embryos exhibit exencephaly. Nature genetics. 1995;10(2):175-80.

699 30. Armstrong JF, Kaufman MH, Harrison DJ, Clarke AR. High-frequency developmental
700 abnormalities in p53-deficient mice. Curr Biol. 1995;5(8):931-6.

701 31. Kim U, Kim CY, Oh H, Lee JM, Chang SN, Ryu B, et al. Phenotyping analysis of p53
702 knockout mice produced by gene editing and comparison with conventional p53 knockout
703 mice. Genes Genomics. 2019;41(6):701-12.

704 32. Tateossian H, Morse S, Simon MM, Dean CH, Brown SD. Interactions between the otitis
705 media gene, Fbxo11, and p53 in the mouse embryonic lung. Dis Model Mech.
706 2015;8(12):1531-42.

707 33. Venkatachalam S, Shi YP, Jones SN, Vogel H, Bradley A, Pinkel D, et al. Retention of
708 wild-type p53 in tumors from p53 heterozygous mice: reduction of p53 dosage can promote
709 cancer formation. EMBO J. 1998;17(16):4657-67.

710 34. de Andrade KC, Lee EE, Tookmanian EM, Kesserwan CA, Manfredi JJ, Hatton JN, et al.
711 The TP53 Database: transition from the International Agency for Research on Cancer to the
712 US National Cancer Institute. Cell Death Differ. 2022;29(5):1071-3.

713 35. Elies L, Guillaume E, Gorieu M, Neves P, Schorsch F. Historical Control Data of
714 Spontaneous Pathological Findings in C57BL/6J Mice Used in 18-Month Dietary
715 Carcinogenicity Assays. Toxicol Pathol. 2024;52(2-3):99-113.

716 36. Cooper TK, Meyerholz DK, Beck AP, Delaney MA, Piersigilli A, Southard TL, et al.
717 Research-Relevant Conditions and Pathology of Laboratory Mice, Rats, Gerbils, Guinea Pigs,
718 Hamsters, Naked Mole Rats, and Rabbits. ILAR J. 2021;62(1-2):77-132.

719 37. Truett GE, Heeger P, Mynatt RL, Truett AA, Walker JA, Warman ML. Preparation of
720 PCR-quality mouse genomic DNA with hot sodium hydroxide and tris (HotSHOT).
721 Biotechniques. 2000;29(1):52, 4.

722 38. Jinadasa R, Balmus G, Gerwitz L, Roden J, Weiss R, Duhamel G. Derivation of thymic
723 lymphoma T-cell lines from Atm(-/-) and p53(-/-) mice. J Vis Exp. 2011(50).

724 39. Heldin A, Cancer M, Palomar-Siles M, Ohlin S, Zhang M, Sun-Zhang A, et al. Novel
725 compounds that synergize with aminoglycoside G418 or eRF3 degraders for translational
726 readthrough of nonsense mutant TP53 and PTEN. RNA Biol. 2023;20(1):368-83.

727

728

729 **Figure legends**

730

731 **Figure 1. Generation of the *Trp53*^{R210X} knock-in mouse strain. (A)** Schematic
732 representation of the CRISPR/Cas9 strategy for generation of *Trp53*^{R210X} mutant mice.
733 A single-guide RNA (sgRNA) was designed to target the region encoding the R210
734 codon in *Trp53* exon 6. The expected cleavage site is 3 nucleotides upstream of the
735 Protospacer Adjacent Motif (PAM) sequence. The donor single-stranded
736 oligodeoxynucleotide (ssODN) template was designed to introduce nucleotide
737 replacements resulting in an Arg (CGC) to STOP (TGA) substitution (indicated in red)
738 at codon 210 (R210X), and an XbaI cut site to facilitate genotyping by restriction
739 enzyme digestion (introduced nucleotide shown in green). Silent mutations introduced
740 to prevent recutting of the sgRNA are shown in orange. The figure is not to scale. **(B)**
741 Representative results from sequence analysis of plasmid clones from edited NIH/3T3
742 cell clones, showing a correct R210X sequence but inconsistent introduction of the
743 XbaI site. **(C)** Genotyping strategy using wildtype (WT) and mutation specific primers
744 for PCR amplification. PCR products were run on a 2% agarose gel. WT allele is
745 identified by a 95 bp PCR fragment (top panel), and mutant allele by a 252 bp PCR
746 fragment (bottom panel). **(D)** Representative chromatograms showing clean WT
747 (upper panel) and mutated (lower panel) *Trp53* sequences from heterozygous F1 mice,
748 indicating successful knock-in of desired mutations and germline transmission of the
749 R210X allele. Altered nucleotides producing the STOP codon (TGA) at amino acid
750 position 210 are shown in red, silent mutations are shown in orange.

751

752 **Figure 2. Female *Trp53*$^{R210X/R210X}$ mice are significantly lighter, and *Trp53*^{R210X}**
753 **mice have a reduced lifespan.** Bodyweight development of female **(A)** and male **(B)**

754 *Trp53*$^{R210X/+}$ and *Trp53*$^{R210X/R210X}$ mice as compared to wildtype (WT) littermates. **(A)**
755 Female *Trp53*$^{R210X/R210X}$ mice were significantly lighter during their whole lifespan as
756 compared to *Trp53*$^{R210X/+}$ and WT littermates (****$p < 0.0001$). **(B)** Male mice of the
757 different genotypes showed no bodyweight differences until 34 weeks of age. From
758 this point, at the end of their maximum lifespan, male *Trp53*$^{R210X/R210X}$ mice were
759 significantly lighter than *Trp53*$^{R210X/+}$ and WT littermates (****$p < 0.0001$). Indicated *n*-
760 values are the total number of mice monitored from 2 weeks of age. Only weights from
761 mice scored as healthy according to general health assessment are shown in **A-B**, as
762 a mouse with tumor burden tends to either dramatically lose weight or gain weight. **(C-**
763 **E)** Kaplan-Meier curves illustrating the effects of the *Trp53*^{R210X} mutation on survival.
764 WT littermates and *Trp53*^{R172H} missense mutant *Trp53* knock-in mice are shown for
765 comparison. All inter-strain comparisons between different genotypes of both
766 *Trp53*^{R210X} and *Trp53*^{R172H} strains were highly significant (adj. P-values: ***$p < 0.001$)
767 (WT vs heterozygous; WT vs homozygous; heterozygous vs homozygous); only P-
768 values for comparison of *Trp53*$^{R210X/+}$ and *Trp53*$^{R172H/+}$ mice are indicated in the figure.
769 **(C)** Male *Trp53*$^{R210X/+}$ mice showed significantly longer survival compared to
770 *Trp53*$^{R172H/+}$ mice (adj. P-value: *$p < 0.05$), but the difference between the female
771 heterozygous mice of the two strains was not statistically significant **(D)**. **(E)** When
772 male and female mouse survival data were combined, *Trp53*$^{R210X/+}$ mice lived
773 significantly longer than *Trp53*$^{R172H/+}$ mice (adj. P-value: **$p < 0.01$). There was no
774 difference in the survival between *Trp53*$^{R210X/R210X}$ and *Trp53*$^{R172H/R172H}$ mice of either
775 gender, or when data for male and female mice were combined. **(F-G)** Comparison of
776 male and female survival of the different genotypes showed only a significant
777 difference for *Trp53*$^{R210X/+}$ mice (**$p < 0.01$). Black ticks in panels **C-G** indicate mice
778 that have been censored (i.e. euthanized due to non-cancer related reasons such as

779 wounds from scratching/over-grooming or malocclusion). Bodyweight growth curves in
780 **A** and **B** were analyzed by Mixed-effects analysis with Tukey's multiple comparisons
781 test. Values represent the mean ± SEM. Survival curves in **C-G** were analyzed by log-
782 rank (Mantel-Cox) test followed by correction for multiple comparisons using the Holm-
783 Šídák method when applicable (**C-E**). P-values: *$p < 0.05$, **$p < 0.01$, ***$p < 0.001$,
784 ****$p < 0.0001$.
785
786 **Figure 3. *Trp53*$^{R210X/R210X}$ mice develop spontaneous tumors with frequent**
787 **metastases.** Examples of tumors observed at necropsy and their histopathological
788 diagnosis. All necropsy photographs are oriented with the head at the top. All
789 histomicrographs are stained with hematoxylin-eosin (HE). Scale bars = 20μm. Red
790 stars indicate mitotic figures. **(A1)** A male *Trp53*$^{R210X/R210X}$ mouse with a severely
791 enlarged thymus (T). **(A2)** Histomicrograph of the thymus neoplasia in A1. The normal
792 thymus architecture is completely effaced by mats of neoplastic round cells with
793 dispersed tangible body macrophages phagocytosing dead neoplastic cells (arrows).
794 The neoplastic lymphocytes were confirmed as CD3-positive, i.e. T-cells
795 (Supplementary table S4). **(A3)** Histomicrograph of lung shown in A1 with moderate
796 perivascular neoplastic lymphocyte infiltrate (metastases, M) in the hilus, L indicates
797 unaffected lung tissue. **(B1)** A male *Trp53*$^{R210X/R210X}$ mouse with a severely enlarged
798 spleen (S) and liver (Li). **(B2)** Histomicrograph of spleen shown in B1. The normal
799 splenic architecture is completely effaced by mats of neoplastic round cells, confirmed
800 as T-cells (CD3-positive) (Supplementary table S4). **(B3)** Histomicrograph of liver
801 shown in B1, with severe perivascular and intrasinusoidal neoplastic lymphocyte
802 infiltrates (metastases), Li indicates remnants of liver parenchyma with hepatocytes,
803 and V indicates vessel lumen. **(C1)** A male *Trp53*$^{R210X/R210X}$ mouse with a

804 subcutaneous tumor on the left side of thorax and abdomen. **(C2)** Histomicrograph of
805 the subcutaneous tumor in C1, with a dense proliferation of pleomorphic neoplastic
806 mesenchymal cells forming streams and bundles. Arrow indicates a giant cell with a
807 bizarre, giant nucleus. Immunohistochemistry confirmed that the neoplastic cells
808 originated from skeletal muscle (Supplementary table S4). **(D)** Distribution of tumors
809 and metastasizing tumors in *Trp53*$^{R210X/R210X}$ mice. The total number of mice includes
810 all mice with at least one tumor.
811
812 **Figure 4. *Trp53*$^{R210X/+}$ mice develop a wide spectrum of tumors with frequent LOH**
813 **and high rate of metastases.** Examples of tumors observed at necropsy and their
814 histopathological diagnosis. All necropsy photographs are oriented with the head at
815 the top. All histomicrographs are stained with hematoxylin-eosin (HE). Scale bars =
816 20µm. Red stars indicate mitotic figures. **(A1)** A female *Trp53*$^{R210X/+}$ mouse with a hard
817 tumor (O = osteosarcoma) on the thorax wall, involving several ribs. **(A2)**
818 Histomicrograph of the hard tumor in A1, with dense proliferation of very pleomorphic,
819 neoplastic round to spindle-shaped mesenchymal cells that produce variable amounts
820 of neoplastic osteoid (arrows), confirming osteosarcoma diagnosis. **(A3)**
821 Histomicrograph of lung from the animal shown in A1, with a large intravascular
822 osteosarcoma metastasis (IvO) adhering to the vessel wall (arrows = neoplastic
823 osteoid, L = lung parenchyma, Alv = alveolus). **(B1)** A male *Trp53*$^{R210X/+}$ mouse with a
824 pale, multinodulated and severely enlarged liver (Li). Insets show an enlarged, pale
825 thymus (T) *in situ*, and the normal-sized spleen (S) after removal from the abdomen,
826 with a pale neoplasia at one pole. **(B2)** Histomicrograph of liver from the animal shown
827 in B1, with dense proliferations of pleomorphic, round neoplastic mesenchymal cells
828 i.e. a soft-tissue sarcoma. (Li = liver parenchyma). **(B3)** Histomicrograph of thymus

829 shown in B1, with infiltrates of neoplastic mesenchymal cells (soft-tissue sarcoma
830 metastases) (Hc = Hassals corpuscule in the thymic parenchyma). **(B4)**
831 Histomicrograph of spleen shown in B1, with a soft-tissue sarcoma metastasis (Srp =
832 splenic red pulp). **(C1)** A male *Trp53*$^{R210X/+}$ mouse with numerous severely enlarged
833 peripheral lymph nodes (Submand L = submandibular, Ax L = axillar, and Ing L =
834 inguinal lymph nodes). Inset shows lungs *in situ.* **(C2 and C3)** Histomicrographs of a
835 lymph node and the spleen from the animal shown in C1, with dense proliferation of
836 neoplastic round cells variably effacing the normal tissue architecture i.e. lymphoma.
837 **(C4-C6)** Histomicrographs of lung, liver and kidney from the animal shown in C1, with
838 perivascular and interstitial neoplastic infiltrates, i.e. metastatic lymphoma (**C4**: Alv =
839 alveolus, V = blood vessel lumen, L = lung parenchyma; **C5**: Li = liver parenchyma;
840 **C6**: Ki = kidney parenchyma). **(D)** Distribution and combinations of tumors and
841 metastasizing tumors found in *Trp53*$^{R210X/+}$ mice. The total number of mice includes all
842 mice with at least one tumor. Benign tumors and tumors not further defined were all in
843 animals with at least one other tumor and are thus not shown separately in the pie
844 chart (L = lymphoma; STS = soft-tissue sarcoma; OS = osteosarcoma; C = carcinoma;
845 Met = metastasized). **(E)** Representative agarose gel for evaluation of LOH in tumors
846 from four different mice. Each animal's tail was used as a control tissue. WT (upper
847 panel) and R210X (lower panel) gel band intensities were measured to quantify the
848 percentage of WT allele retained in each tumor compared to the tail; percentage of
849 retained WT allele in each sample is indicated at the bottom of the panel. LOH was
850 defined as <50% WT allele retained. N = no LOH; Y = LOH.
851
852 **Figure 5. *Trp53*$^{R210X/R210X}$ mice show a higher rate of thymic lymphomas and**
853 **lymphoma metastases than *Trp53*$^{R210X/+}$ and WT mice, and only *Trp53*$^{R210X/+}$ mice**

854 **develop osteosarcomas which are more frequent in female mice. (A)**
855 *Trp53*$^{R210X/R210X}$ mice developed more lymphomas and lymphoma metastases than
856 *Trp53*$^{R210X/+}$ and WT mice, and *Trp53*$^{R210X/+}$ was the only genotype that had
857 osteosarcomas. All three genotypes developed soft-tissue sarcomas to a similar
858 extent, and with the exception of benign tumors, which were more often found in WT
859 mice, *Trp53*$^{R210X/+}$ and WT mice had similar occurrence of the remaining tumor types.
860 **(B)** *Trp53*$^{R210X/R210X}$ had thymic lymphoma more often than *Trp53*$^{R210X/+}$ and WT mice,
861 but less frequent lymph node lymphomas. All three genotypes showed similar
862 occurrence of splenic lymphomas. **(C)** Comparison of the different combinations of
863 lymphoma sites, without and with metastases, showed that only *Trp53*$^{R210X/R210X}$ mice
864 had metastatic thymic lymphoma. *Trp53*$^{R210X/R210X}$ mice also had significantly fewer
865 lymphomas in spleen and/or lymph nodes without metastases, whereas metastases in
866 these sites occurred in all three genotypes at a similar rate (differences not statistically
867 significant). **(D)** A gender effect on tumor type presentation was only found in
868 *Trp53*$^{R210X/+}$ mice, where osteosarcoma was more common in female mice and soft-
869 tissue sarcoma more common in male mice. *Trp53*$^{R210X/R210X}$ and WT mice showed no
870 significant differences between genders (Supplementary Fig. S2). **(E-G)** A male
871 *Trp53*$^{R210X/R210X}$ mouse was sacrificed at 234 days of age due to weight loss, strained
872 breath and a neoplasia on the throat, and subjected to an *ex vivo* MRI analysis without
873 prior necropsy. **(E and F)** The throat neoplasia was part of a large neoplastic thymus
874 (outlined by yellow arrows, size approx. 2.7x1.3x0.9 cm) that intrathoracally extended
875 caudally to the diaphragm (indicated by a white arrow in **E**), cranially through the
876 thoracic inlet along the ventral neck to the level of the ramus mandibularis, and
877 extending into the right-side musculature medial to the shoulder, probably involving the
878 prescapular lymph node. In the right cranial mediastinum there was a neoplastically

879 transformed cranial mediastinal lymph node, about 0.8 cm long and 0.4 cm in diameter.
880 The submandibular lymph nodes were not identifiable and appeared to be continuous
881 with the thymus tumor. The lungs had a clear appearance with no signs of neoplastic
882 proliferations or infiltrates. **(G)** In the dorsal abdomen there were multiple enlarged
883 lymph nodes, up to 3 mm in diameter, elongated and convoluted (outlined by white
884 arrows). The spleen was mildly enlarged and rounded (not shown), and in the normal-
885 sized liver there were two nodules with an appearance best consistent with areas of
886 vacuolar degeneration and extramedullary hyperplasia. Differences between
887 genotypes in **A-C** were analyzed with Kruskal-Wallis test, followed by Dunn's multiple
888 comparisons test. Differences between genders in **D** were analyzed with Mann
889 Whitney U test. P-values: *$p < 0.05$, **$p < 0.001$; ****$p < 0.0001$.
890
891 **Figure 6. Metastasis has no effect on overall survival of *Trp53*$^{R210X/R210X}$ and**
892 ***Trp53*$^{R210X/+}$ mice whereas tumor site (thymus) and size affect survival of**
893 ***Trp53*$^{R210X/R210X}$ mice. (A)** Kaplan-Meier curves illustrating the impact of metastasis on
894 survival of *Trp53*$^{R210X/R210X}$ and *Trp53*$^{R210X/+}$ mice. Metastatic disease did not change
895 survival in *Trp53*$^{R210X/R210X}$ mice. *Trp53*$^{R210X/+}$ mice with metastases showed a
896 significantly delayed time until declared moribund but not altered overall survival. Data
897 for *Trp53*$^{R210X/+}$ mice may be skewed by the reduced survival of mice with
898 osteosarcoma, as this group only included two cases with metastases (not shown). **(B)**
899 *Trp53*$^{R210X/R210X}$ mice with thymic lymphomas had reduced survival compared to mice
900 with splenic and/or lymph node lymphomas regardless of metastatic status. **(C)** The
901 solitary thymic lymphomas were larger than thymic lymphomas that were concurrent
902 with other lymphomas or soft-tissue sarcomas; adjusted P-values are shown. **(D)**
903 *Trp53*$^{R210X/R210X}$ mice with solitary thymic lymphomas showed the shortest overall

904 survival. Survival curves in **A, B** and **D** were analyzed by log-rank (Mantel-Cox) test;
905 in **D** all survival curves were compared to the group with solitary thymic lymphoma. **C**:
906 all groups were compared to the solitary thymic lymphoma group using One-way
907 ANOVA followed by Dunnett's multiple comparisons tests. P-values: *$p < 0.05$, **$p <$
908 0.001; ***$p < 0.001$.
909
910 **Figure 7. G418 induces translational readthrough and full-length functional p53**
911 **in *Trp53*$^{R210X/R210X}$ T-lymphoma cells. (A)** Representative histomicrographs of the
912 thymus from the *Trp53*$^{R210X/R210X}$ mouse X405 stained with HE (left) and CD3 antibody
913 (IHC, right). Mats of CD3-positive, i.e. T-cell origin, pleomorphic neoplastic
914 lymphocytes and dispersed, moderate numbers of tangible body macrophages (left
915 panel, arrows) efface the normal thymic architecture. Scale bars = 50µm. **(B)**
916 Representative flow cytometry to verify T-cell origin of the X405 *Trp53*$^{R210X/R210X}$ T-
917 lymphoma cell line established from a thymic lymphoma by staining with antibodies for
918 CD3 (left panel), and CD4 and CD8 (right panel). **(C)** Immunofluorescence staining of
919 X405 *Trp53*$^{R210X/R210X}$ T-lymphoma cells, either untreated (NT, upper panels) or treated
920 with 100µM G418 (lower panels) for 72 hours. p53 was detected using N1 (N-terminal
921 epitope) and 280aa C-term (C-terminal epitope) antibodies. Rightmost panels show
922 merged DAPI and 280aa C-term p53 staining, highlighting translational readthrough of
923 the *Trp53*-R210X nonsense mutation and production of full-length p53 protein upon
924 treatment with G418. Scale bars = 100µm. **(D)** Western blot analysis showing dose-
925 dependent induction of full-length p53 in X405 *Trp53*$^{R210X/R210X}$ T-lymphoma cells
926 following 72h treatment with G418. p53 was visualized using the anti-p53 antibody
927 1C12 that recognizes an N-terminal epitope and therefore detects both full-length and
928 C-terminally truncated p53. Gapdh was used as a loading control. **(E)** qRT-PCR

929 analysis showing dose-dependent induction of *p53* mRNA levels in X405
930 *Trp53*$^{R210X/R210X}$ T-lymphoma cells after 72h treatment with G418. mRNA levels of p53
931 target genes *p21*, *Puma* and *Zmat3* were significantly upregulated upon treatment with
932 200μM G418. Gene expression values were normalized to *Gapdh* expression and
933 compared to the untreated (NT) negative control. **(F)** Representative flow cytometry
934 for assessment of cell death by Annexin V staining of X405 *Trp53*$^{R210X/R210X}$ T-
935 lymphoma cells (left) and quantification of 3 flow cytometry replicates (right), showing
936 significant increase in cell death following treatment with 200μM G418 for 72h. In **E-F**:
937 statistical analysis was performed using one-way ANOVA followed by Dunnett's **(E)** or
938 Tukey's **(F)** multiple comparisons tests. Values represent the mean ± SEM. Adjusted
939 P-values: *$p < 0.05$, **$p < 0.01$, ***$p < 0.001$, ****$p < 0.0001$.
940

Figure 1

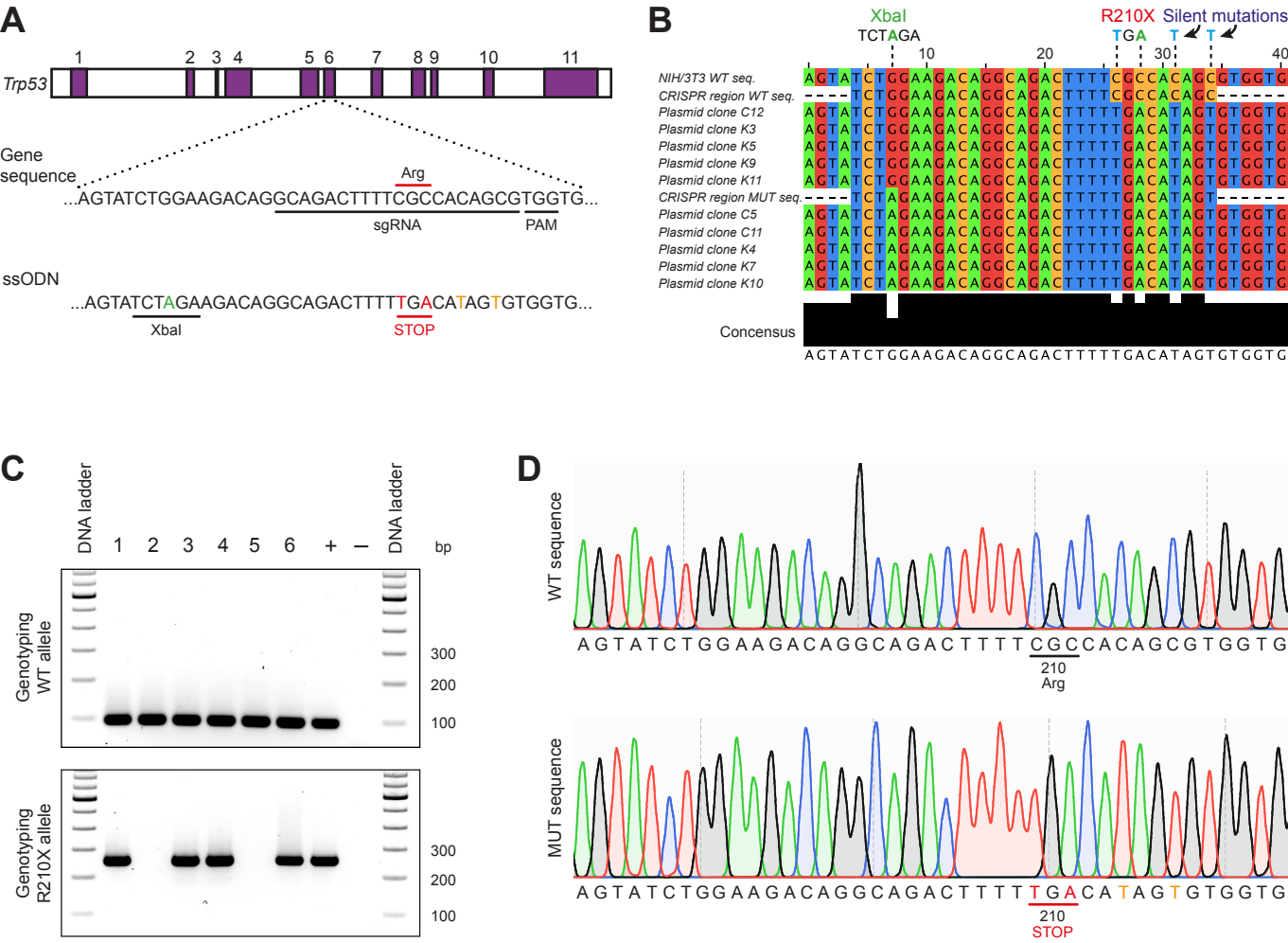
A
Trp53
1 2 3 4 5 6 7 8 9 10 11
Gene sequence
Arg
...AGTATCTGGAAGACAGGCAGACTTTTCGCCACAGCGTGGTG...
sgRNA
PAM
ssODN
...AGTATCTAGAAGACAGGCAGACTTTTTGACATAGTGTGGTG...
XbaI
STOP
B
XbaI
TCTAGA
R210X
TGA
Silent mutations
T T
10 20 30 40
NIH/3T3 WT seq.
CRISPR region WT seq.
Plasmid clone C12
Plasmid clone K3
Plasmid clone K5
Plasmid clone K9
Plasmid clone K11
CRISPR region MUT seq.
Plasmid clone C5
Plasmid clone C11
Plasmid clone K4
Plasmid clone K7
Plasmid clone K10
Concensus
AGTATCTGGAAGACAGGCAGACTTTTTGACATAGTGTGGTG
C
DNA ladder
1 2 3 4 5 6 + –
DNA ladder
bp
Genotyping WT allele
300
200
100
Genotyping R210X allele
300
200
100
D
WT sequence
AGTATCTGGAAGACAGGCAGACTTTTCGCCACAGCGTGGTG
210
Arg
MUT sequence
AGTATCTGGAAGACAGGCAGACTTTTTGACATAGTGTGGTG
210
STOP

Figure 2

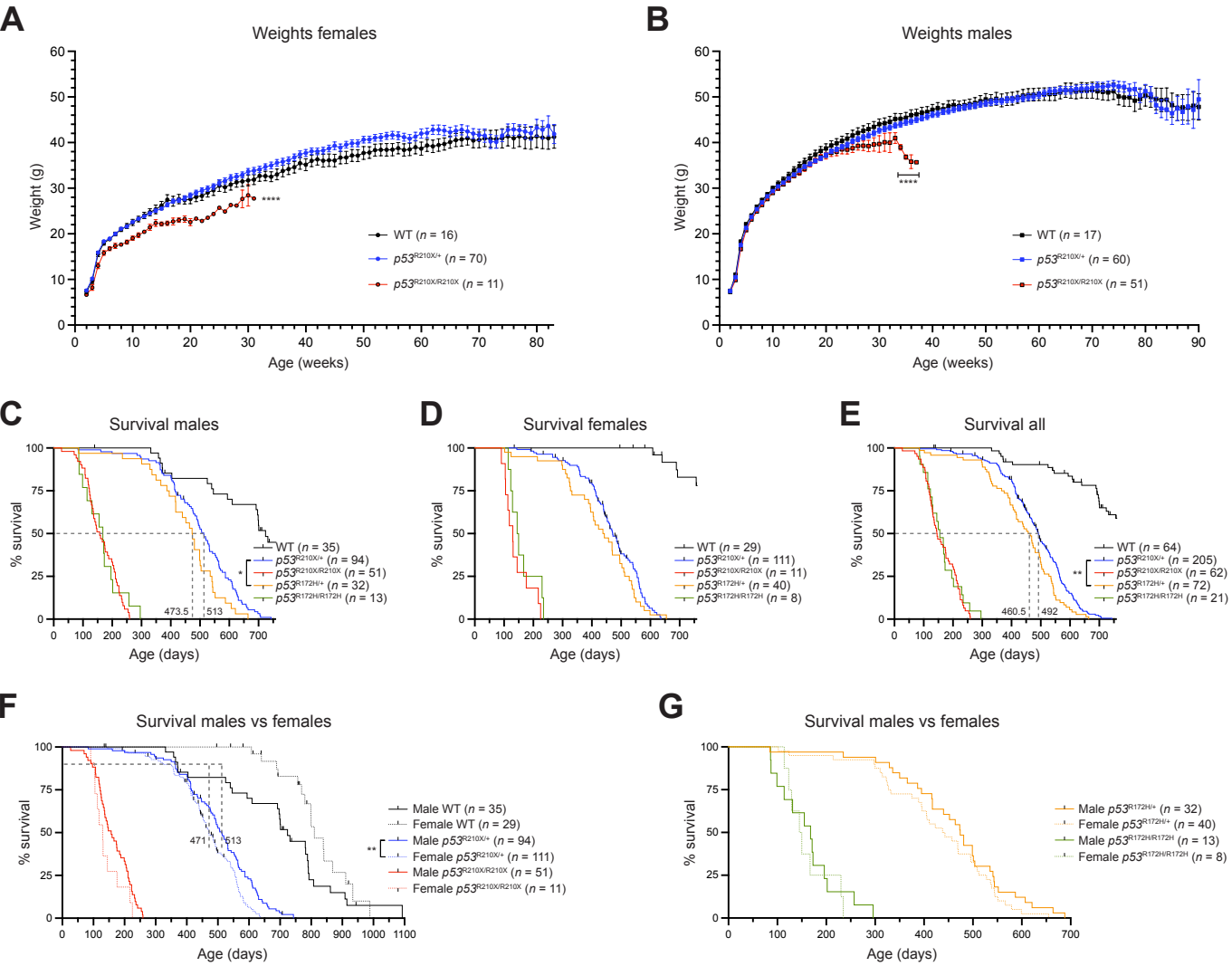
A
Weights females
Weight (g)
Age (weeks)
****
WT (n = 16)
p53R210X/+ (n = 70)
p53R210X/R210X (n = 11)
B
Weights males
Weight (g)
Age (weeks)
****
WT (n = 17)
p53R210X/+ (n = 60)
p53R210X/R210X (n = 51)
C
Survival males
% survival
Age (days)
473.5
513
*
WT (n = 35)
p53R210X/+ (n = 94)
p53R210X/R210X (n = 51)
p53R172H/+ (n = 32)
p53R172H/R172H (n = 13)
D
Survival females
% survival
Age (days)
WT (n = 29)
p53R210X/+ (n = 111)
p53R210X/R210X (n = 11)
p53R172H/+ (n = 40)
p53R172H/R172H (n = 8)
E
Survival all
% survival
Age (days)
460.5
492
**
WT (n = 64)
p53R210X/+ (n = 205)
p53R210X/R210X (n = 62)
p53R172H/+ (n = 72)
p53R172H/R172H (n = 21)

F
Survival males vs females
% survival
Age (days)
471
513
**
Male WT (n = 35)
Female WT (n = 29)
Male p53R210X/+ (n = 94)
Female p53R210X/+ (n = 111)
Male p53R210X/R210X (n = 51)
Female p53R210X/R210X (n = 11)
G
Survival males vs females
% survival
Age (days)
Male p53R172H/+ (n = 32)
Female p53R172H/+ (n = 40)
Male p53R172H/R172H (n = 13)
Female p53R172H/R172H (n = 8)

Figure 3

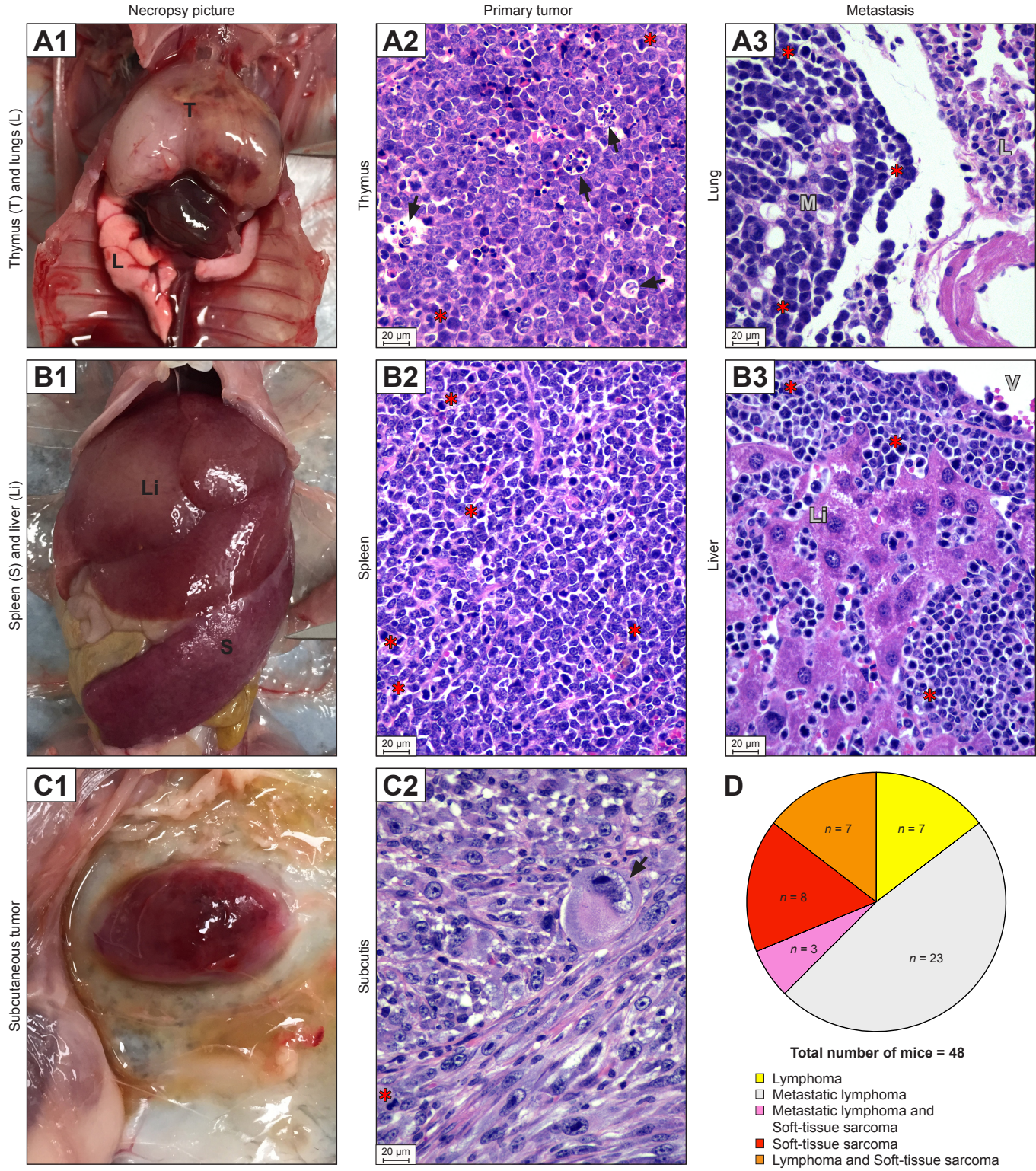
Necropsy picture
Primary tumor
Metastasis
A1
A2
A3
Thymus (T) and lungs (L)
Thymus
Lung
T
L
M
20 µm
B1
B2
B3
Spleen (S) and liver (Li)
Spleen
Liver
Li
S
V
C1
C2
Subcutaneous tumor
Subcutis
D
n = 7
n = 7
n = 8
n = 3
n = 23
Total number of mice = 48
Lymphoma
Metastatic lymphoma
Metastatic lymphoma and Soft-tissue sarcoma
Soft-tissue sarcoma
Lymphoma and Soft-tissue sarcoma

Figure 4

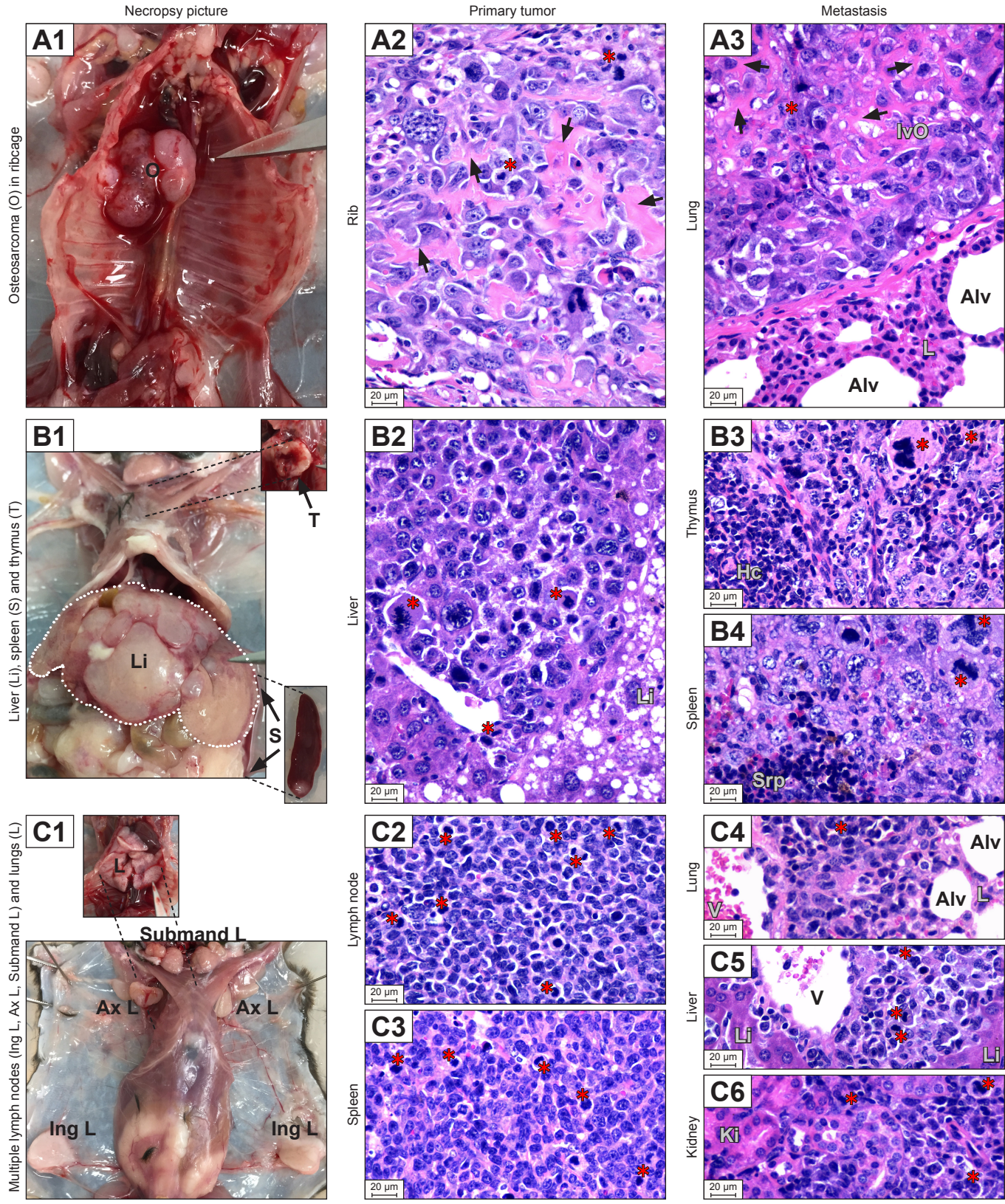
Necropsy picture
Primary tumor
Metastasis
A1
Osteosarcoma (O) in ribcage
O
A2
Rib
20 µm
A3
Lung
IvO
Alv
L
Alv
20 µm
B1
Liver (Li), spleen (S) and thymus (T)
T
Li
S
B2
Liver
Li
20 µm
B3
Thymus
Hc
20 µm
B4
Spleen
Srp
20 µm
C1
Multiple lymph nodes (Ing L, Ax L, Submand L) and lungs (L)
L
Submand L
Ax L
Ax L
Ing L
Ing L
C2
Lymph node
20 µm
C3
Spleen
20 µm
C4
Lung
Alv
Alv
L
V
20 µm
C5
Liver
V
Li
Li
20 µm
C6
Kidney
Ki
20 µm

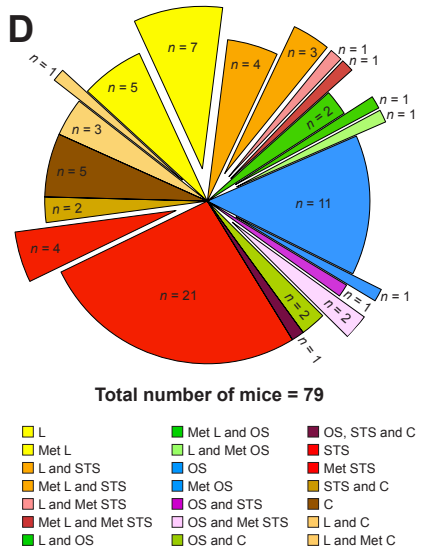
D
n = 7
n = 5
n = 4
n = 3
n = 1
n = 1
n = 1
n = 1
n = 2
n = 3
n = 5
n = 2
n = 11
n = 4
n = 21
n = 1
n = 2
n = 2
n = 1
n = 1
Total number of mice = 79
L
Met L
L and STS
Met L and STS
L and Met STS
Met L and Met STS
L and OS
Met L and OS
L and Met OS
OS
Met OS
OS and STS
OS and Met STS
OS and C
OS, STS and C
STS
Met STS
STS and C
C
L and C
L and Met C

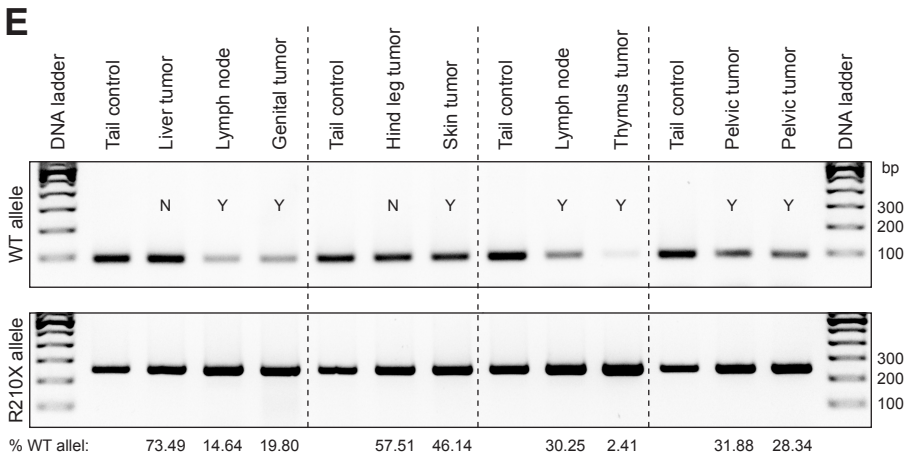
E
DNA ladder
Tail control
Liver tumor
Lymph node
Genital tumor
Tail control
Hind leg tumor
Skin tumor
Tail control
Lymph node
Thymus tumor
Tail control
Pelvic tumor
Pelvic tumor
DNA ladder
bp
WT allele
N
Y
Y
N
Y
Y
Y
Y
300
200
100
R210X allele
300
200
100
% WT allel:
73.49
14.64
19.80
57.51
46.14
30.25
2.41
31.88
28.34

Figure 5

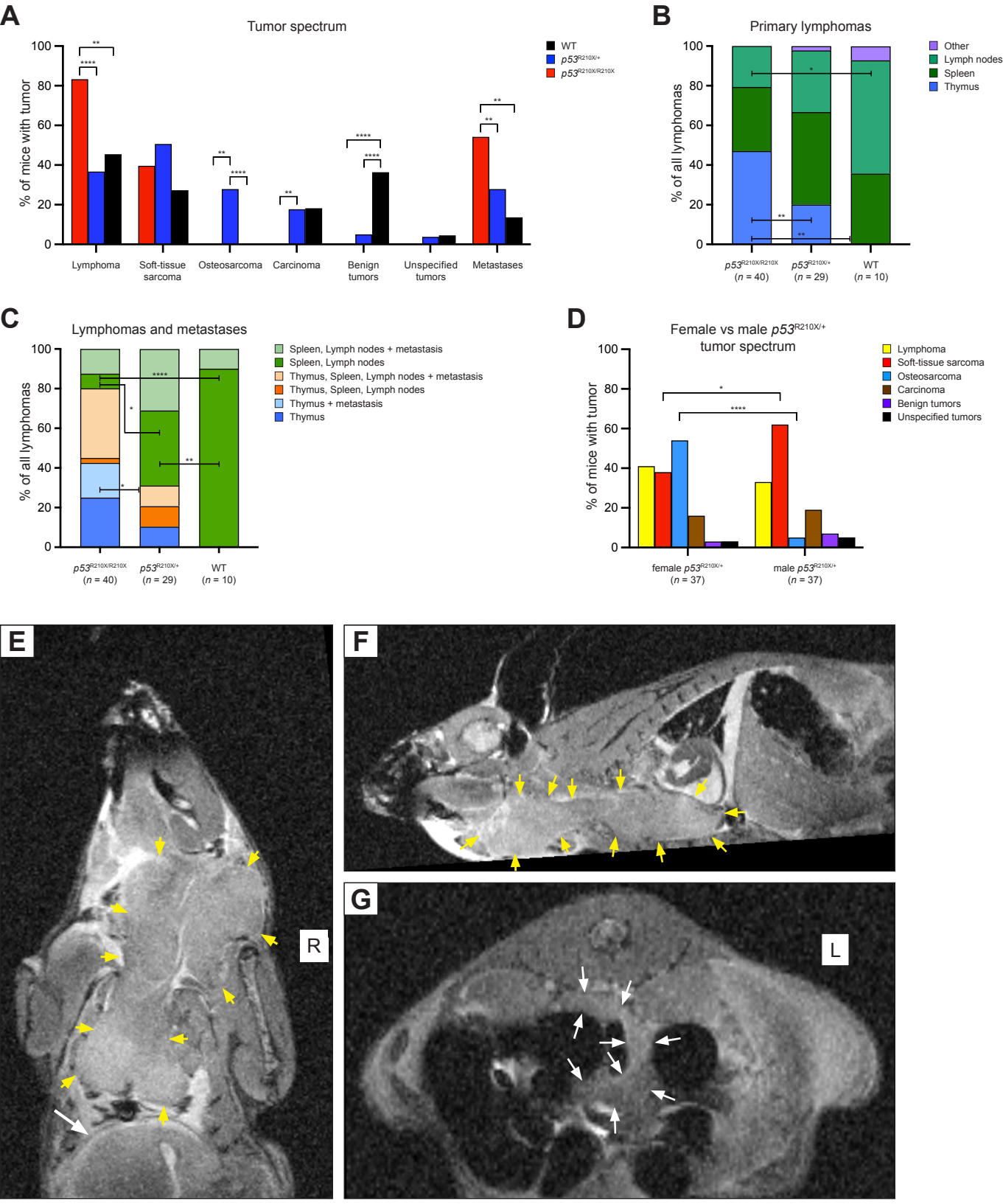
A
Tumor spectrum
% of mice with tumor
WT
p53R210X/+
p53R210X/R210X
Lymphoma
Soft-tissue sarcoma
Osteosarcoma
Carcinoma
Benign tumors
Unspecified tumors
Metastases
B
Primary lymphomas
% of all lymphomas
Other
Lymph nodes
Spleen
Thymus
p53R210X/R210X (n = 40)
p53R210X/+ (n = 29)
WT (n = 10)
C
Lymphomas and metastases
% of all lymphomas
Spleen, Lymph nodes + metastasis
Spleen, Lymph nodes
Thymus, Spleen, Lymph nodes + metastasis
Thymus, Spleen, Lymph nodes
Thymus + metastasis
Thymus
p53R210X/R210X (n = 40)
p53R210X/+ (n = 29)
WT (n = 10)
D
Female vs male p53R210X/+ tumor spectrum
% of mice with tumor
Lymphoma
Soft-tissue sarcoma
Osteosarcoma
Carcinoma
Benign tumors
Unspecified tumors
female p53R210X/+ (n = 37)
male p53R210X/+ (n = 37)
E
R
F
G
L

Figure 6

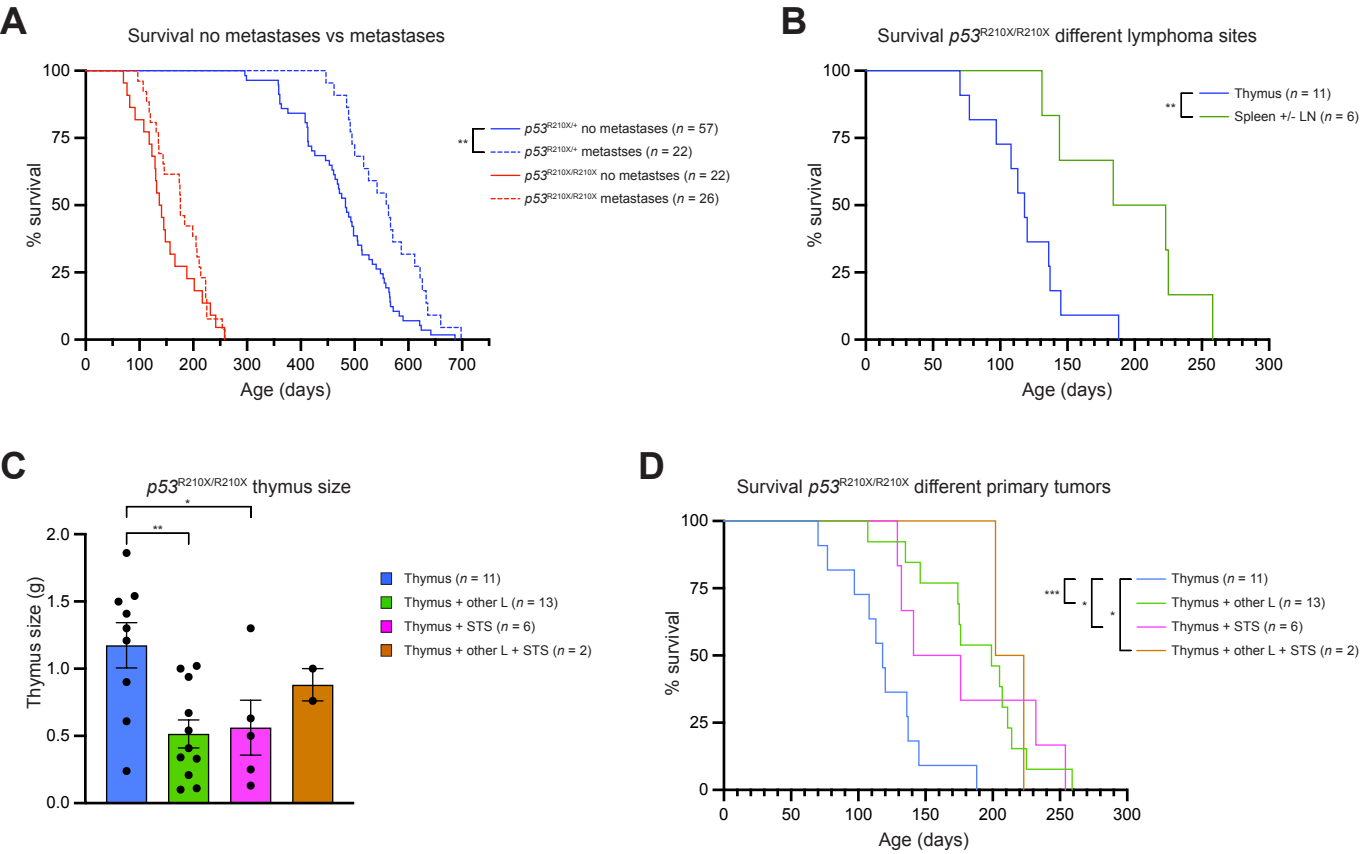
A
Survival no metastases vs metastases
% survival
Age (days)
**
p53R210X/+ no metastases (n = 57)
p53R210X/+ metastses (n = 22)
p53R210X/R210X no metastses (n = 22)
p53R210X/R210X metastases (n = 26)
B
Survival p53R210X/R210X different lymphoma sites
% survival
Age (days)
**
Thymus (n = 11)
Spleen +/- LN (n = 6)
C
p53R210X/R210X thymus size
Thymus size (g)
*
**
Thymus (n = 11)
Thymus + other L (n = 13)
Thymus + STS (n = 6)
Thymus + other L + STS (n = 2)
D
Survival p53R210X/R210X different primary tumors
% survival
Age (days)
***
*
*
Thymus (n = 11)
Thymus + other L (n = 13)
Thymus + STS (n = 6)
Thymus + other L + STS (n = 2)

Figure 7

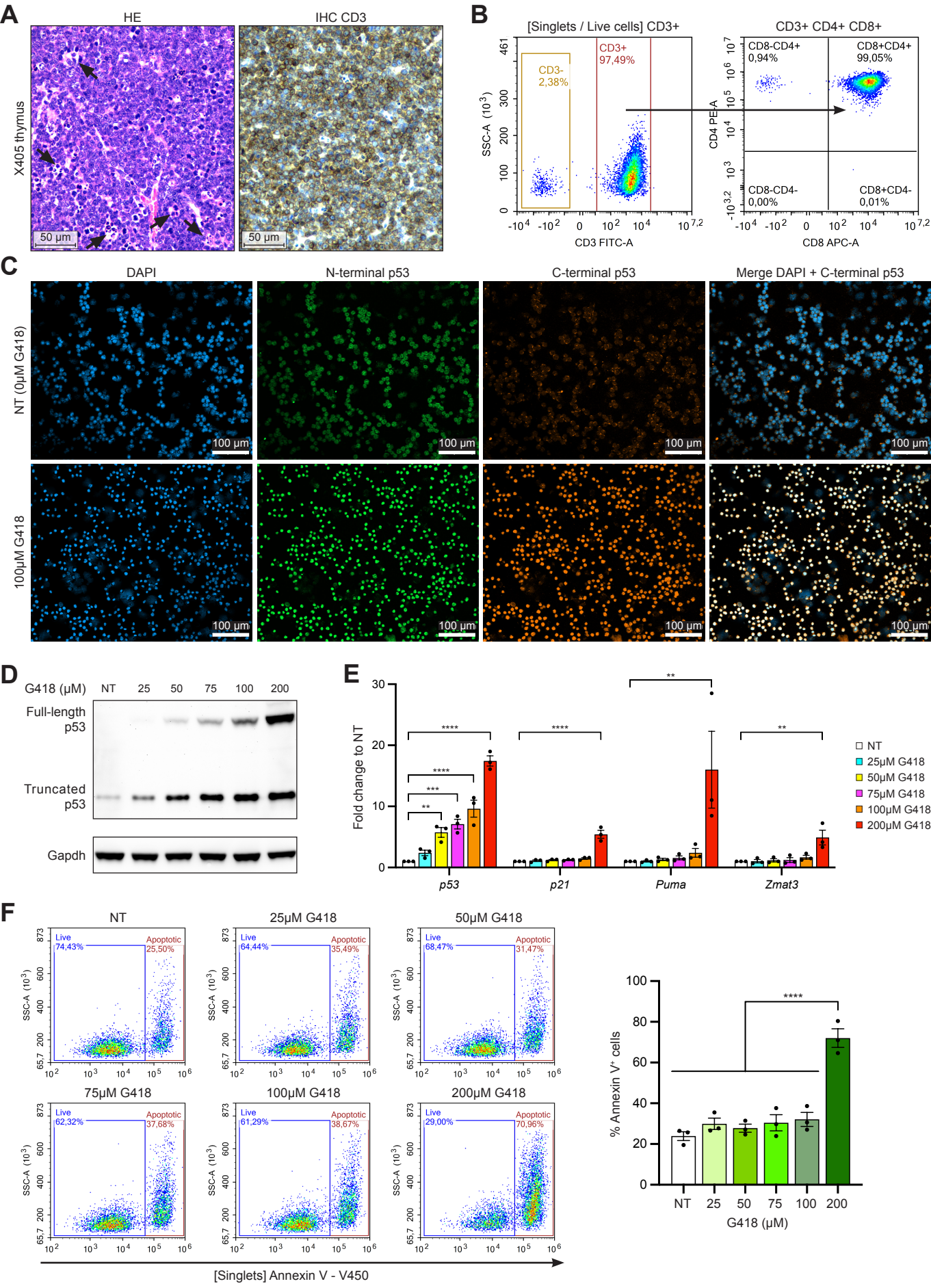
A
HE
IHC CD3
X405 thymus
50 µm
50 µm
B
[Singlets / Live cells] CD3+
CD3+ CD4+ CD8+
CD3-
2,38%
CD3+
97,49%
SSC-A (10^3)
CD3 FITC-A
CD8-CD4+
0,94%
CD8+CD4+
99,05%
CD8-CD4-
0,00%
CD8+CD4-
0,01%
CD4 PE-A
CD8 APC-A
C
DAPI
N-terminal p53
C-terminal p53
Merge DAPI + C-terminal p53
NT (0µM G418)
100µM G418
100 µm
D
G418 (µM)
NT
25
50
75
100
200
Full-length p53
Truncated p53
Gapdh
E
Fold change to NT
NT
25µM G418
50µM G418
75µM G418
100µM G418
200µM G418
p53
p21
Puma
Zmat3
F
NT
25µM G418
50µM G418
75µM G418
100µM G418
200µM G418
Live
Apoptotic
74,43%
25,50%
64,44%
35,49%
68,47%
31,47%
62,32%
37,68%
61,29%
38,67%
29,00%
70,96%
SSC-A (10^3)
[Singlets] Annexin V - V450
% Annexin V+ cells
G418 (µM)